The effect of streamwise braid vortices on the particle dispersion in a plane mixing layer. I. Equilibrium points and their stability

B. Marcu and E. Meiburg[a)]
Department of Aerospace Engineering, University of Southern California, Los Angeles, California 90089-1191

(Received 8 June 1995; accepted 25 October 1995)

The dynamics of small, heavy, spherical particles are investigated in an analytical model of the stretched counterrotating streamwise braid vortices commonly found in three-dimensionally evolving mixing layers. The flow field consists of two superimposed rows of Stuart vortices of opposite sign, with an additional two-dimensional strain field. The particle dynamics are determined by a balance of inertial, gravitational, and viscous drag forces, i.e., the dimensionless Stokes and Froude numbers, St and Fr, as well as by the dimensionless strain rate, and the Stuart vortex family parameter. Equilibrium points for the particles, as well as their stability criteria, are determined analytically, both in the absence and in the presence of gravity, and for different orientations of the gravity vector. In the absence of gravity, accumulation of low St particles can occur at the center of the braid vortices. An analytical expression for the critical particle diameter, below which accumulation is possible, is derived. The presence of gravity can lead to the emergence of multiple equilibrium points, whose stability properties depend on their locations. For a horizontal mixing layer flow and strong gravity effects, unconditional accumulation can occur midway between the streamwise braid vortices in the upwelling regions. Conditionally stable accumulation regions exist a short horizontal distance away from the centers of the braid vortices. If the gravity vector lies within the plane of the mixing layer, accumulation points exist only for moderate strengths of gravity. Under these circumstances, conditional accumulation is possible near the streamwise vortex centers. © *1996 American Institute of Physics.* [S1070-6631(96)00303-6]

I. INTRODUCTION

Due to its importance in a variety of technical applications and environmental contexts, particle dispersion in plane mixing layers has been the focus of a considerable amount of recent experimental and computational research. The main thrust of this work has been towards understanding and quantifying the role played by the two-dimensional large-scale coherent vortices,[1] which are triggered by a Kelvin-Helmholtz instability and dominate the flow by means of a succession of vortex pairing events.[2] As was first pointed out by Crowe, Gore, and Troutt,[3] these coherent vortices preferentially disperse particles whose ratio of aerodynamic response time to characteristic flow time, also known as the particle Stokes number, is on the order of unity. This finding was subsequently confirmed and extended both by further two-dimensional computational studies,[4–7] as well as by experimental investigations.[8–12] These studies demonstrate that the main mechanism for the dispersion of particles into the unseeded stream consists of their ejection from the vortex centers, and the subsequent formation of bands of high particle accumulations near the free stagnation point in the braid region between consecutive Kelvin-Helmholtz rollers. There these bands become aligned with the direction of extensional strain, which subsequently pulls them into the unseeded free stream. Scaling arguments presented by Martin and Meiburg[6] as well as Raju and Meiburg[7] show this accumulation process to be optimally effective for a particle Stokes number of one.

All of the above two-dimensional investigations draw attention to the importance of the braid region in the particle dispersion process. The crucial role played by this region near the free stagnation point then immediately raises the question as to how the two-dimensional scenario for the particle dispersion mechanism is modified by the presence of the three-dimensional secondary vortex structure known to exist in this part of the flow field. These counterrotating coherent streamwise vortices[13–15] arise through the reorientation of the initially weak spanwise braid vorticity into the streamwise direction. Subsequently they undergo strong stretching in the extensional strain field created by the evolving spanwise Kelvin-Helmholtz vortices. As a result, they can reach considerable strength, and their associated velocity field plays an important role in the three-dimensional evolution of the flow. A detailed computational investigation of the formation and subsequent evolution of this streamwise vortex structure in the mixing layer was undertaken by Corcos and Lin.[16] Subsequently, Lin and Corcos[17] presented numerical computations for a quasi-two-dimensional model of the strained streamwise braid vorticity that demonstrates how the self-induced velocity of the regions of opposite-signed streamwise vorticity, in conjunction with the extensional plane strain, can lead to the collapse of the streamwise vorticity into concentrated vortex tubes. The computations, as well as the asymptotic analysis by Neu,[18] show that the collapsed, concentrated streamwise vorticity tubes under plane strain acquire a structure which can be approximated by that

[a)]Corresponding author: Department of Aerospace Engineering, University of Southern California, Los Angeles, California 90089-1191. Phone: 213-740-5376, fax: 213-740-7774.

of axisymmetric Burgers vortices[19] in axisymmetric strain.

With respect to the dynamics of heavy particles, these three-dimensional attributes of the flow field in the braid region raise issues that are absent from the two-dimensional mixing layer. In particular, Marcu, Meiburg, and Newton[20] recently demonstrated the possibility of particle trapping in a Burgers vortex, since the centrifugal ejection of the particle by the vortex can be counteracted by the inward pointing viscous drag created by the strain component of the velocity vector. They formulated and solved the corresponding stability problem, which led to an analytical criterion for particle trapping. It was furthermore shown that in the presence of gravity multiple equilibrium points can exist, which, if stable, lead to the accumulation of particles. This demonstrates that the inclusion of the secondary vortex structure in the braid region can lead to entirely new dynamical effects in the particle behavior. The counteracting effects of centrifugal ejection caused by the streamwise vortices and compressive strain induced by the Kelvin-Helmholtz structures provide the key mechanisms for an overall complex dynamical behavior of the particles. It will be of interest to investigate the possibility of trapping and accumulation in such an array of streamwise vortices under plane strain, and the extent to which these or other new features of particle dynamics modify the purely two-dimensional scenario.

The most complete quantitative data on particle dispersion in three-dimensionally evolving mixing layers will eventually be provided by three-dimensional direct numerical simulations and experimental measurements. However, the interpretation, understanding, and ultimately the modeling of such data has to be built on insight gained from the qualitative and quantitative analysis of simplified flow models that allow us to study the interaction of several important mechanisms in isolation. It is in this spirit, which proved to be so successful in the investigations by Lin and Corcos[17] and Neu,[18] that we intend to elucidate the mechanisms by which the counterrotating strained streamwise vortex tubes in the braid region influence the dispersion of heavy particles in three-dimensionally evolving mixing layers. For this purpose, we will introduce a model of the fluid flow in the braid region that captures the essential features of the real flow. This flow model, as well as the governing equations for the particle dynamics, is presented in section II of this paper, along with a discussion of its advantages and shortcomings in comparison with potential alternate models. The parameters that enter into this model are furthermore interpreted from the point of view of experimental situations, in order to establish a connection between the two. In Section III we analyze this model with respect to the existence of equilibrium points. Their stability characteristics are evaluated in order to establish whether or not they can serve as accumulation points for the particles. In Section IV we extend the analysis to include gravity as well. Finally, in section V we summarize the results and discuss their implications for the particle dispersion process. It should be pointed out that the above *linear* results concern only the existence and stability of equilibrium points. Issues such as the *nonlinear* dynamics of particles, or the size of the basin of attraction of the equilibrium points, will be addressed by means of numerical simulations, to be discussed in Part 2 of the present investigation.[21] There we will focus on the potential accumulation of particles at equilibrium points or on equilibrium trajectories, along with the characteristic features of the particle concentration fields, in order to gain insight into the relevant transport mechanisms for particles that do not collect at stable equilibrium points, and to quantify particle concentration distributions.

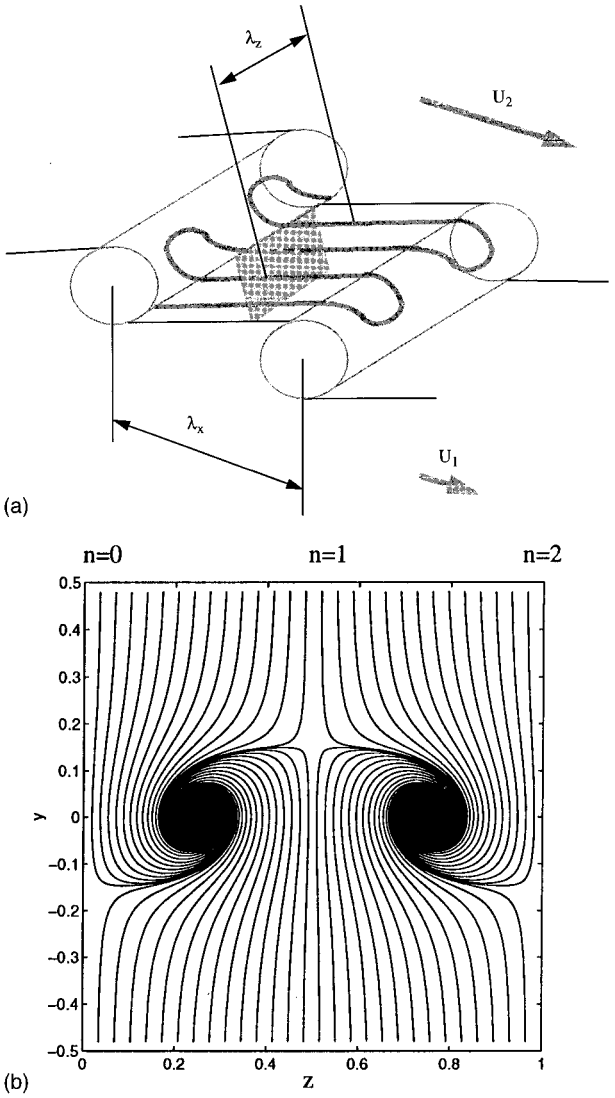

FIG. 1. (a) The three-dimensional Bernal-Roshko shear layer model: λ_x is the spacing between the spanwise vortices and λ_z is the spacing between two vortices with the same direction of vorticity in the row of counterrotating vortices. (b) Streamlines for the row of counterrotating vortices in the cross-stream z,y-plane for $\sigma=4.0$ and $k=0.9$

II. FLOW MODEL

A. Fluid velocity field

Our goal is to investigate the dynamics of heavy particles in the z,y-plane across the braid region of a plane mixing layer [Fig. 1(a)]. For this purpose, we follow Lin and Corcos[17] in approximating the flow as being quasi-two-dimensional. In this way, the effect of the compressive strain due to the spanwise Kelvin-Helmholtz vortices can be ac-

counted for, but any variation in the streamwise x-direction is neglected. After rendering all spatial coordinates, velocity components, time, and pressure dimensionless by referring them to a characteristic length l^* and a characteristic velocity u^*, respectively, the steady incompressible continuity and Navier-Stokes equations take the form

$$\frac{\partial v}{\partial y}+\frac{\partial w}{\partial z}=-\sigma, \tag{1}$$

$$v\,\frac{\partial v}{\partial y}+w\,\frac{\partial v}{\partial z}=-\frac{\partial p}{\partial y}+\frac{1}{Re}\left(\frac{\partial^2 v}{\partial y^2}+\frac{\partial^2 v}{\partial z^2}\right), \tag{2}$$

$$v\,\frac{\partial w}{\partial y}+w\,\frac{\partial w}{\partial z}=-\frac{\partial p}{\partial z}+\frac{1}{Re}\left(\frac{\partial^2 w}{\partial y^2}+\frac{\partial^2 w}{\partial z^2}\right), \tag{3}$$

l^* and u^* will be specified below. Here

$$\sigma=\frac{\partial u}{\partial x} \tag{4}$$

denotes the strength of the plane strain and

$$\mathbf{U}=\mathbf{i}\sigma x+\mathbf{j}v+\mathbf{k}w \tag{5}$$

represents the fluid velocity vector. In order to obtain the flow in the cross-stream z,y-plane, we have to make a fundamental choice. One possibility is to solve the above equations numerically, in a way similar to Lin and Corcos.[17] The advantage of this approach is that it gives a solution which, except for truncation errors of the selected computational algorithm, accurately satisfies these equations. The flow field can then be seeded with heavy particles in order to study different aspects of their behavior such as accumulation, dispersion, etc. The disadvantage of this strategy lies in the difficulty to obtain information in an analytical form, which could be useful in the development of simplified models and scaling laws. For example, the limits of stability for conditionally stable equilibrium points as a function of the particle Stokes number would be hard to obtain, as would be the location of unstable equilibrium points. For these purposes, it would be preferable to employ an analytical model of the fluid flow in the z,y-plane. Such a model will allow us to make progress analytically towards determining the location of equilibrium points, their respective stability criteria, etc. However, due to the nonlinearity of the governing system of equations, no model for this flow is known that satisfies equations (1)–(3) exactly. In spite of this obvious shortcoming, it is our belief that an investigation based on a simplified analytical model should precede a full numerical simulation of the problem, as it allows us to develop insight and intuition which will be useful in conducting and interpreting direct simulations of the governing equations.

The particular flow model that we choose is based on the solution to the steady two-dimensional Euler equations known as Stuart vortices.[22] This solution describes a periodic row of like-signed vortices a distance λ_z apart from each other. The vortex row separates two free streams with a difference velocity ΔW. By taking λ_z as the characteristic length l^* and ΔW as the characteristic velocity u^*, we obtain for the dimensionless streamfunction of the Stuart vortices,

$$\psi=\frac{1}{4\pi}\ln[\cosh(2\pi(y-y_0))-k\,\cos(2\pi(z-z_0))], \tag{6}$$

where (z_0,y_0) denotes the location of a vortex center. The parameter k determines the degree to which the vorticity is concentrated in the vortex cores. For $k=1$, the flow is that induced by a row of corotating point vortices, while for $k=0$ we have a uniform shear layer with a tanh velocity profile.

The above streamfunction describes the flow field due to a row of corotating vortices. In order to obtain a model for a counterrotating vortex row, we superimpose another Stuart vortex row of equal strength and opposite sign, whose vortex centers are located midway between the vortices of the original row at (z_1,y_1). To account for the plane strain, we furthermore add a fluid velocity component,

$$v_s=-\sigma y, \tag{7}$$

where σ denotes the dimensionless strain rate, which is related to the dimensional strain $\tilde{\sigma}$ by

$$\sigma=\tilde{\sigma}\,\frac{\lambda_z}{\Delta W}. \tag{8}$$

Due to the strain component, the fluid velocity field in the z,y-plane no longer is divergence free, so that it cannot be expressed in terms of a streamfunction. The dimensionless velocity components, which are periodic in the spanwise z-direction, then have the form

$$w_f=-0.5\,\frac{\sinh[2\pi(y-y_0)]}{\cosh[2\pi(y-y_0)]-k\,\cos[2\pi(z-z_0)]}+0.5\,\frac{\sinh[2\pi(y-y_1)]}{\cosh[2\pi(y-y_1)]-k\,\cos[2\pi(z-z_1)]}, \tag{9}$$

$$v_f=0.5\,\frac{k\,\sin[2\pi(z-z_0)]}{\cosh[2\pi(y-y_0)]-k\,\cos[2\pi(z-z_0)]}-0.5\,\frac{k\,\sin[2\pi(z-z_1)]}{\cosh[2\pi(y-y_1)]-k\,\cos[2\pi(z-z_1)]}-\sigma y. \tag{10}$$

It should be noted that far away from the counterrotating vortex row the horizontal velocity component now approaches zero. However, even though ΔW thus can no longer be interpreted as a free stream velocity difference, it still serves to characterize the strength of the counterrotating vortices.

The above velocity components solve the continuity equation (1) exactly. However, while they satisfy the inviscid form of the governing momentum equations (2),(3) for $k=1$, this is not the case for other values of k, due to the nonlinearity of those equations. The error increases for smaller values of k, so that the following analysis is more accurate the closer k is to unity. It should be mentioned that Mallier and Maslowe[23] recently gave a closed form solution to the steady incompressible Euler equations for a row of counterrotating vortices, based on a streamfunction derived from a complex potential suggested by Milne-Thomson. Still, when subjected to plane strain, this flow field as well fails to solve the governing equations exactly. By setting $z_0=0.25$, $y_0=0$ and $z_1=0.75$, $y_1=0$, we place the vortices on the z-axis such that

we have a counterclockwise rotating vortex at $z=0.25$, and a clockwise rotating one at $z=0.75$. For illustrative purposes, streamlines are shown in Fig. 1(b) for $k=0.9$ and $\sigma=4$. The vortex centers correspond to foci in the streamline plot, indicating their sink-like character due to the plane strain, which is compressive in the y-direction and extensional in the x-direction. Apart from the vortex centers, we find further fixed points at locations z,y defined by

$$z=\pm\frac{n}{2},$$
$$(-1)^{n+1}\,\frac{k}{\cosh(2\pi y)}-\sigma y=0. \tag{11}$$

These equilibrium points represent saddle points. Even values of n, and $n=0$ in particular, indicate free stagnation points below the z-axis in the downwelling regions, whereas odd values of n denote those above the z-axis in the upwelling regions.

The natural scaling for the present quasi-two-dimensional problem is based on the spanwise period λ_z and on ΔW, which characterizes the strength of each streamwise vortex. In a typical experimental flow, however, the circulation of the streamwise vortices $\Gamma_x\simeq\Delta W\lambda_z$ increases with time. During the initial, nearly two-dimensional evolution of a transitional mixing layer, the streamwise vortices are quite weak, but during the later stages their circulation can grow to the same order as that of the spanwise Kelvin-Helmholtz vortices $\Gamma_z\simeq\Delta U\lambda_x$. Here, ΔU denotes the streamwise velocity difference between the two streams forming the mixing layer, and λ_x indicates the spacing of the Kelvin-Helmholtz vortices. During these later stages of the three-dimensional evolution, the dimensional strain $\tilde{\sigma}$ stays approximately constant. Its strength is estimated[24] as

$$\tilde{\sigma}\sim 3\,\frac{\Delta U}{\lambda_x}. \tag{12}$$

By rendering this strain dimensionless in the way described earlier, i.e., with ΔW and λ_z, we obtain

$$\sigma\sim 3\,\frac{\Delta U\lambda_z}{\Delta W\lambda_x}, \tag{13}$$

so that

$$\sigma\sim 3\,\frac{\Gamma_z}{\Gamma_x}\left(\frac{\lambda_z}{\lambda_x}\right)^2. \tag{14}$$

Bernal and Roshko[13] find that typically $\lambda_z/\lambda_x=2/3$. Thus, the minimum dimensionless strain rates that we should consider, corresponding to the stage where the streamwise vortices have reached a strength that is of the same order as that of the spanwise vortices, is approximately $\sigma=4/3$.

In summary, motivated by the desire to make analytical progress, we apply a simplified quasi-two-dimensional model for the fluid velocity field. This model consists of two superimposed rows of counterrotating Stuart vortices residing in a plane strain field. In this way, the model reproduces the periodic array of counterrotating stretched stream-wise braid vortices known to dominate the braid region of nominally two-dimensional mixing layers. While it satisfies the continuity equation identically for all values of the Stuart family parameter k, the model represents an exact solution to the Euler equations only in the limit $k\to 1$. However, even for values of k near unity the structure of the model vortices approaches that of axisymmetric Burgers vortices, just as solutions to the full Navier-Stokes solutions do.[17,18] It should be pointed out that the model is time-independent, so that the dynamic roll-up of the initially weak streamwise braid vorticity is not reproduced.

B. Equation of motion for the particles

We limit our investigation to the dilute regime, in which the particle concentration is small enough for the interaction among particles and the effect of the particle motion on the fluid flow to be neglected. We furthermore consider only particles whose density ρ_p is much greater than that of the surrounding fluid ρ_f, such as solid particles or liquid drops in gaseous flows. Under these conditions, the particle motion is dominated by the effects of particle inertia, the viscous drag force created by the slip velocity, and gravity.[8] The velocity $\mathbf{V}_p=(w_p,v_p)$ and location x_p of a small spherical particle of diameter d in the fluid velocity field $\mathbf{U}=(w_f,v_f)$ are then governed by the dimensionless equations[25]

$$\frac{d\mathbf{V}_p}{dt}=\frac{1}{St}\,(\mathbf{U}|_{\mathbf{x}=\mathbf{x}_p}-\mathbf{V}_p)+\frac{1}{Fr^2}\,\mathbf{e}_g, \tag{15}$$

$$\frac{d\mathbf{x}_p}{dt}=\mathbf{V}_p, \tag{16}$$

where we have applied Stokes' drag law, based on the assumption of small particle Reynolds numbers.[26] Here $\mathbf{e}_g$ represents the unit vector in the direction of the projection of gravity on the z,y-plane. Note that, as a consequence of the quasi-two-dimensional nature of the flow field, in conjunction with Stokes' drag law, the motion of the particles in the spanwise and cross-stream directions is decoupled from that in the streamwise x-direction. The dimensionless parameters,

$$St=\frac{d^2\rho_p\Delta W}{18\rho_f\nu_f\lambda_z} \tag{17}$$

and

$$Fr=\frac{\Delta W}{\sqrt{\lambda_z g}}, \tag{18}$$

are the Stokes and Froude numbers, respectively. Here ν_f denotes the kinematic viscosity of the fluid and g represents the length of the projection of gravity on the z,y-plane, so that the above equations hold for all orientations of gravity. Notice that, as a result of the above scaling, the Stokes number St of a particle will vary as ΔW or λ_z change during the evolution of the flow field. As is well known, St indicates the ratio of the particle's aerodynamic response time and the characteristic flow time scale. Small values of St correspond to very light particles or relatively viscous fluid, so that the particle motion is dominated by viscous forces, and the particle can be expected to follow the fluid closely. For heavy particles or less viscous fluids, on the other hand, St takes large values, and the particle motion becomes mostly a func-

tion of its inertia. Here Fr expresses in dimensionless form the relative importance of inertial and gravitational forces. As Fr decreases, gravity becomes more important for the dynamical behavior of the particle.

It is of interest to compare the particle Stokes number values caused by the spanwise Kelvin-Helmholtz vortices with those due to the streamwise braid vortices. The flow time scale t_{stream} corresponding to the Kelvin-Helmholtz vortices is given by λ_x^2/Γ_z. On the other hand, the flow time scale t_{span} imposed by the streamwise vortices can be written as λ_z^2/Γ_x. With $\lambda_z \approx 2/3\lambda_x$[13] and $\Gamma_x \approx 1/2\Gamma_z$,[27] we obtain $t_{\text{stream}} \approx 9/8 t_{\text{span}}$, leading us to conclude that, by the time the streamwise vortices have reached a mature stage, the two time scales are of the same order. This indicates that those particles that are preferentially concentrated in the braid region by the Kelvin-Helmholtz vortices will also be strongly influenced by the streamwise braid vortices.

We can write equations (15) and (16) as a nonlinear four-dimensional system for z_p, y_p, w_p, and v_p,[28] obtaining

$$\dot{\mathbf{x}} = \mathbf{F}(x), \tag{19}$$

where

$$\mathbf{x} = \begin{bmatrix} z_p \\ y_p \\ w_p \\ v_p \end{bmatrix}, \quad \mathbf{F}(x) = \begin{bmatrix} w_p \\ v_p \\ \dfrac{1}{St}(w_f - w_p) + \dfrac{e_{gz}}{Fr^2} \\ \dfrac{1}{St}(v_f - v_p) + \dfrac{e_{gy}}{Fr^2} \end{bmatrix}. \tag{20}$$

Here e_{gz} and e_{gy} represent the z- and y-components of the unit vector in the direction of the z,y-projection of the gravity vector. This system of ordinary differential equations with appropriate initial conditions specified for $t=0$ constitutes a nonlinear dissipative dynamical system.

III. EQUILIBRIUM POINTS AND THEIR STABILITY IN THE ABSENCE OF GRAVITY

In the absence of gravity, the only equilibrium points for the particles are the stagnation points given by (11) and the centers of the counterrotating vortices. The stagnation points are saddle points, as indicated by the streamline pattern in Fig. 1, so that they are unstable for particle accumulation.[20] In the following, we analyze the linear stability at the center of the vortex located at $z=0.25$, $y=0$.

The fluid velocity field (9),(10) can be linearized around the vortex center by obtaining a series expansion form for the horizontal and vertical velocities, retaining only the first order terms in the expansions of the hyperbolic and trigonometric functions,

$$\begin{aligned} w_f &= \frac{2\pi k}{1-k^2}\, y\left[2\pi^2 \frac{1+k^2}{1-k^2}(z-z_0)^2 - 1\right], \\ v_f &= \frac{2\pi k}{1-k^2}(z-z_0)\left[1 - 2\pi^2 \frac{1+k^2}{1-k^2}(z-z_0)^2\right] - \sigma y, \end{aligned} \tag{21}$$

We express the expanded equations (21) in coordinates with the origin at the vortex center by making the transformation $\zeta = z - z_0$. Subsequent linearization with respect to y and ζ yields

$$\begin{aligned} w_f &= -\frac{2\pi k}{1-k^2}\, y, \\ v_f &= \frac{2\pi k}{1-k^2}\, \zeta - \sigma y. \end{aligned} \tag{22}$$

Using (22), the particle motion equations in the absence of gravity (19),(20) can be written as

$$\begin{bmatrix} \dot{\zeta}_p \\ \dot{y}_p \\ \dot{w}_p \\ \dot{v}_p \end{bmatrix} = \begin{bmatrix} 0 & 0 & 1 & 0 \\ 0 & 0 & 0 & 1 \\ 0 & -c & -a & 0 \\ c & -b & 0 & -a \end{bmatrix} \begin{bmatrix} \zeta_p \\ y_p \\ w_p \\ v_p \end{bmatrix}, \tag{23}$$

where $a = 1/St$, $b = \sigma/St$, $c = \phi(k)/St$, and $\phi(k) = 2\pi k/(1-k^2)$.

The coefficient matrix of the system (23) has eigenvalues of the form

$$s_{1,2,3,4} = -\frac{1}{St} \pm \frac{1}{St}\sqrt{1 - 2\sigma St \pm 2St\sqrt{\sigma^2 - 4\phi^2(k)}}. \tag{24}$$

The discussion of stability depends on the value of the expression $\sigma^2 - 4\phi^2(k)$. When this expression is negative, all four eigenvalues (24) are complex, with the real part of the form

$$\mathrm{Re}(s) = -\frac{1}{2St} \pm \frac{1}{2St}\,\rho^{1/2}\cos\left(\frac{\theta}{2}\right),$$

where

$$\rho^2 = 1 - 4\sigma St + 16St^2\phi^2(k) \tag{25}$$

and

$$\theta = \tan^{-1}\left(\frac{2St\sqrt{4\phi^2(k) - \sigma^2}}{1 - 2\sigma St}\right). \tag{26}$$

For stability, one requires $\mathrm{Re}(s) < 0$. Using the trigonometric identity,

$$\cos\left(\frac{\theta}{2}\right) = \frac{1}{\sqrt{2}}\sqrt{1 + \frac{1}{\sqrt{1 + \tan^2(\theta)}}}, \tag{27}$$

in isolating the real part of the eigenvalues (24), we obtain the stability condition

$$St \leqslant \frac{2\sigma}{4\phi^2(k) - \sigma^2} = St_{cr}. \tag{28}$$

If $\sigma^2 - 4\phi^2(k)$ is positive, one can show immediately that if

$$1 - 2\sigma St \pm 2St\sqrt{\sigma^2 - 4\phi^2(k)} < 0, \tag{29}$$

the eigenvalues (24) are complex and have negative real parts. If

$$1 - 2\sigma St \pm 2St\sqrt{\sigma^2 - 4\phi^2(k)} \geqslant 0, \tag{30}$$

the eigenvalues are real, and the inequality $s_{1,2,3,4} \leqslant 0$ [where only the "+" signs need to be considered in (24)] leads to

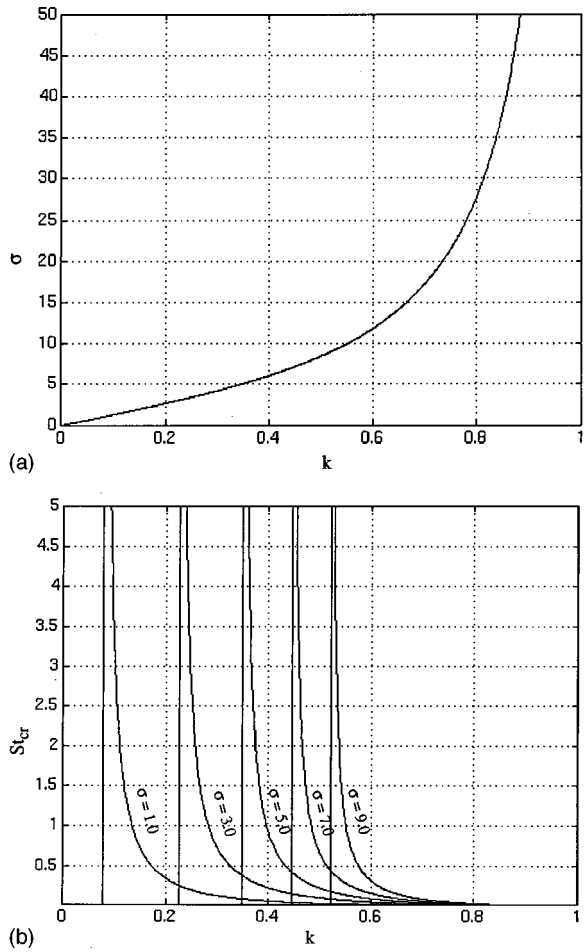

FIG. 2. (a) Variation of the critical σ with respect to k. Above the curve, the equilibrium point is unconditionally stable, while below the curve the stability depends on the St values, as shown in (b). (b) Variation of the critical St with respect to k for different values of the strain parameter σ, as indicated. For each curve the vertical asymptote is shown, below which unconditional stability is achieved.

the condition $16St^2\phi^2(k)\geqslant 0$, which is always satisfied. Thus, in this last case, the eigenvalues (24) are real but will always have nonpositive values.

In summary, the conditions for stability at the center of the vortex are

$$\sigma^2-4\phi^2(k)>0, \text{ stable,}$$

$$\sigma^2-4\phi^2(k)\leqslant 0\begin{cases} St\leqslant \dfrac{2\sigma}{4\phi^2(k)-\sigma^2}, & \text{stable,} \\ St>\dfrac{2\sigma}{4\phi^2(k)-\sigma^2}, & \text{unstable.}\end{cases} \tag{31}$$

The variation of the critical strain parameter with the Stuart family parameter is shown in Fig. 2(a). Above the curve, the equilibrium points are stable, while below the curve the second stability condition in (31) applies. The strain parameter necessary to ensure unconditional stability grows rapidly as k increases. During the initial stages of a typical mixing layer evolution, the streamwise vortex cores are not yet concentrated, so that they correspond to small values of k. The dimensionless strain σ, on the other hand, is quite large. These conditions lie above the curve in Fig. 2(a), and thus correspond to the stable accumulation of particles at the centers of the vortices. As the vortices develop, their cores shrink, forming regions of concentrated vorticity, described by higher values of k. Under these conditions, the strain can balance only the centrifugal forces of smaller and smaller particles, so that it depends on St whether or not particle accumulation occurs.

In the conditional stability zone, below the curve in Fig. 2(a), the critical value St_{cr} drops rapidly with increasing k. In Fig. 2(b), the variation of St_{cr} with k at constant values of σ is shown for $1\leqslant\sigma\leqslant 9$. For each curve, below the k value corresponding to the critical strain curve for a given σ in Fig. 2(a), St_{cr} is infinite. Then, as k increases, St_{cr} decreases rapidly towards zero.

We conclude that diluted streamwise vorticity as well as strong strain is required for stable accumulation of particles at the centers of the vortices. As the vortices are stretched by the axial strain, and their cores achieve concentrated vorticity, only particles characterized by smaller and smaller St can accumulate.

A scaling analysis can relate the particle size to the mixing layer characteristics, based on the set of conditions (31). There, the term $\phi^2(k)$ expresses the non-dimensional vorticity at the center of the vortex, as computed from the linearized velocity field (22). It is the competition between the fluid velocity related to the vorticity and that related to the strain which determines the stability of the particle at the center of the vortex.

The above stability criterion (31) can be used in order to obtain a critical particle size, below which accumulation is possible. To this end, we employ Neu's[18] result that a vortex stretched by plane strain asymptotically approaches an axisymmetric Burgers vortex with a dimensional vorticity distribution,

$$\tilde{\omega}=\frac{\Gamma}{4\pi R^2}\exp\left(-\frac{r^2}{4R^2}\right). \tag{32}$$

Here Γ is the vortex circulation. Also, R denotes the core radius, which asymptotically approaches $R^2=\nu/\tilde{\sigma},\tilde{\sigma}$ being the dimensional plane strain. Thus the vorticity at the vortex center has the value

$$\tilde{\omega}=\frac{\Gamma}{4\pi\nu}\,\tilde{\sigma}. \tag{33}$$

Corcos and Sherman[24] provide a scaling law for the plane strain as $\tilde{\sigma}\sim 3\Delta U/\lambda_x$ where ΔU is the streamwise velocity difference of the mixing layer, and λ_x denotes the spacing between the spanwise Kelvin-Helmholz vortices. By non-dimensionalizing $\tilde{\sigma}$ with λ_z and ΔW, and using Bernal and Roshko's observation[13] that $\lambda_x\sim 3\lambda_z/2$, the non-dimensional strain coefficient becomes

$$\sigma=\frac{2\Delta U}{\Delta W}. \tag{34}$$

Non-dimensionalizing the vorticity (33) in the same way, we obtain, with (34),

$$\omega=\frac{\Gamma}{2\pi\nu}\frac{\Delta U}{\Delta W}. \tag{35}$$

By employing (34) and (35) in (31), the critical St is expressed as

$$St_{cr}=\frac{\frac{\Delta W}{\Delta U}}{(\Gamma/2\pi\nu)^2-1}. \tag{36}$$

From the above expression, one can estimate the critical particle diameter in terms of the characteristic flow parameters. An important scaling result from the experiments of Bernal and Roshko,[13] and Bell and Mehta[27] is that the spacing λ_z of the streamwise vortices scales with the vorticity thickness δ_ω of the mixing layer,

$$\lambda_z \sim \delta_\omega = \frac{\Delta U}{(\partial U/\partial y)_{\max}}. \tag{37}$$

By using (37) and (17) in conjunction with expression (36) for the critical value of St, one obtains an estimate for the critical particle diameter,

$$d_{cr}^2 \sim \frac{\Upsilon}{(\partial U/\partial y)_{\max}[(\Gamma/2\pi\nu)^2-1]}, \tag{38}$$

where $\Upsilon=(18\rho_f\nu_f)/\rho_p$ depends only on the material properties of the particle and the fluid. Notice that the velocity differences ΔU and ΔW no longer appear in the relation above. The expression indicates that for weak vortices accumulation of relatively large particles is possible. For increasing rotational velocities, the diameter of the particles that can accumulate decreases rapidly.

IV. EQUILIBRIUM POINTS AND THEIR STABILITY IN THE PRESENCE OF GRAVITY

A. Gravity perpendicular to the mixing layer

While in the absence of gravity the equilibrium points for the particles were located at the critical points of the fluid velocity field, this is no longer the case when gravity is added. In this section, we assume that the gravity vector points in the $-y$-direction. As a result, the locations of the particle equilibrium points are displaced. Furthermore, additional equilibrium points may be produced.[20] In order to find the coordinates of these points one can use equations (19) and (20) with the particle velocity and acceleration set to zero, along with the fluid velocity field (9),(10). We obtain the following two equations:

$$\begin{aligned}
&-0.5\,\frac{\sinh[2\pi(y-y_0)]}{\cosh[2\pi(y-y_0)]-k\,\cos[2\pi(z-z_0)]}\\
&\quad+0.5\,\frac{\sinh[2\pi(y-y_1)]}{\cosh[2\pi(y-y_1)]-k\,\cos[2\pi(z-z_1)]}=0,\\
&0.5\,\frac{k\,\sin[2\pi(z-z_0)]}{\cosh[2\pi(y-y_0)]-k\,\cos[2\pi(z-z_0)]}\\
&\quad-0.5\,\frac{\sinh[2\pi(z-z_1)]}{\cosh[2\pi(y-y_1)]-k\,\cos[2\pi(z-z_1)]}\\
&\quad-\sigma y-\frac{St}{Fr^2}=0,
\end{aligned} \tag{39}$$

which must be solved for y and z to find the coordinates of the equilibrium points.

It is interesting to note that the equations (39) express the fluid velocity field as given by (9),(10), from which the particle terminal velocity St/Fr^2 has been subtracted. The result is a modified velocity field, whose fixed points represent equilibrium points for the particles.[20] In the absence of gravity, the streamlines of this modified velocity field are identical to the streamlines of the fluid velocity field, shown in Fig. 1(b) for $k=0.9$ and $\sigma=4$. For the same values of k and σ, the streamline patterns of the modified velocity fields for different levels of gravity are shown in Fig. 3. In Fig. 3(a), for $St/Fr^2=0.8$, the foci of the modified velocity field are displaced laterally while the saddle point is significantly displaced downwards, as compared to the no-gravity case. As gravity increase [Fig. 3(b)], two new equilibrium points emerge, located symmetrically with respect to the $z=0.5$ vertical line. Finally, for strong gravity, only one equilibrium point is left, located below the row of vortices on the vertical line $z=0.5$.

An important observation, based on the plots in Fig. 3, is that all equilibrium points are located either on the vertical lines $z=0$ or $z=0.5$, or on the horizontal line $y=0$. The reason for this behavior lies in the fact that only along these lines the horizontal fluid velocity vanishes, which is a necessary condition for the existence of an equilibrium point. This is reflected by the existence of two sets of solutions to the first equation in (39). The first set consists of a family of lines $z=\pm n/2$, along which the equation is satisfied for any y, and the second set represents the line $y=0$, along which the equation is satisfied for any value of z. For convenience, let us denote the first set of solutions as the vertical set, and the second set as the horizontal set.

1. Equilibrium points from the vertical set

By substituting $z=\pm n/2$ into the second equation (39), one obtains an equation for the y-locations along these lines $z=$const, where equilibrium is achieved. The vertical set of solutions for the equilibrium points (z_v, y_v) is given by

$$\begin{aligned}
&z_v=\pm\frac{n}{2},\\
&\frac{(-1)^{n+1}k}{\cosh(2\pi y_v)}-\sigma y_v=\frac{St}{Fr^2}.
\end{aligned} \tag{40}$$

Comparison of this set of points with the stagnation points (11) shows that the equilibrium points of the vertical set are located below the alternating stagnation points (11) of the flow. When $n=1$ (or odd values), i.e., at the periodic z-locations where the fluid is pushed upwards by the vortices, the y_v-coordinate of the equilibrium point can be either positive or negative, depending on the value of the terminal velocity St/Fr^2, but when $n=0$ (or even values), i.e., at the periodic locations where the fluid is pushed downwards by the vortices, the y_v-coordinate of the equilibrium point can only be negative. This fact is important for the stability analysis around the equilibrium points from the vertical set. We will show that the equilibrium points at locations characterized by $n=0$ in (40) are always unstable.

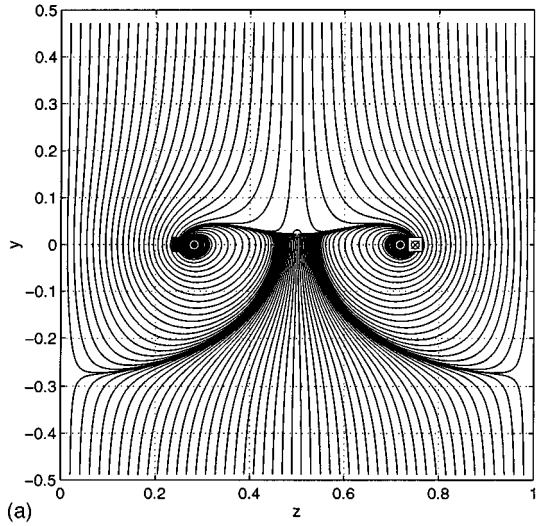

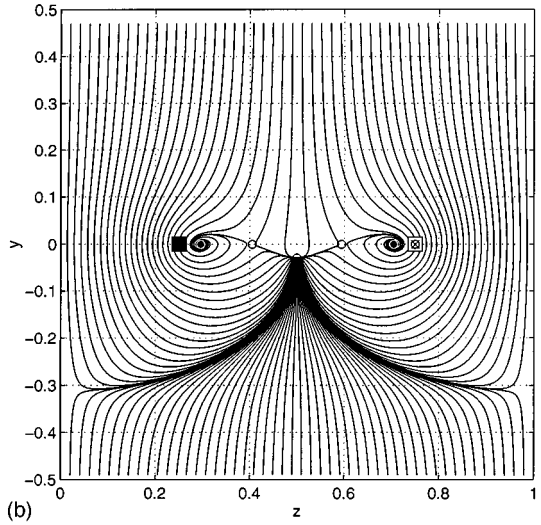

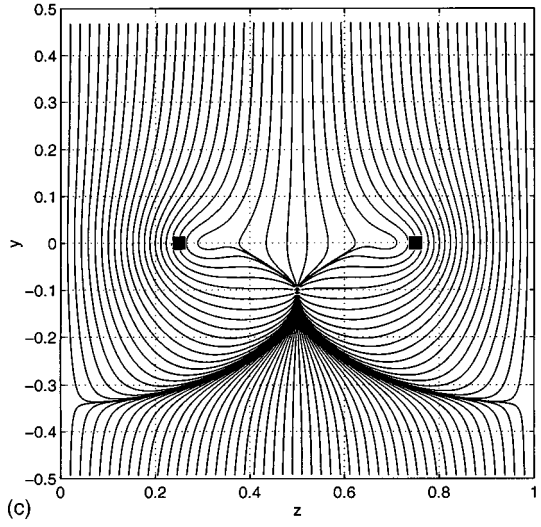

FIG. 3. Modified velocity field for horizontal mixing layers. The square symbols mark the centers of the vortices, while the circles mark the equilibrium points. (a) $\sigma=4.0$; $k=0.9$; $St/Fr^2=0.8$. As gravity increases, the equilibrium points are displaced either laterally, along the vortex row axis, or vertically, along the lines of symmetry between the vortices. (b) $\sigma=4.0$; $k=0.9$; $St/Fr^2=1.0$. As gravity is further increased, the equilibrium points located on the symmetry line between the vortices can be displaced below the line of vortices at $y=0$. (c) $\sigma=4.0$; $k=0.9$; $St/Fr^2=1.15$. For sufficiently strong gravity, only one equilibrium point exists, located significantly below the vortex row line.

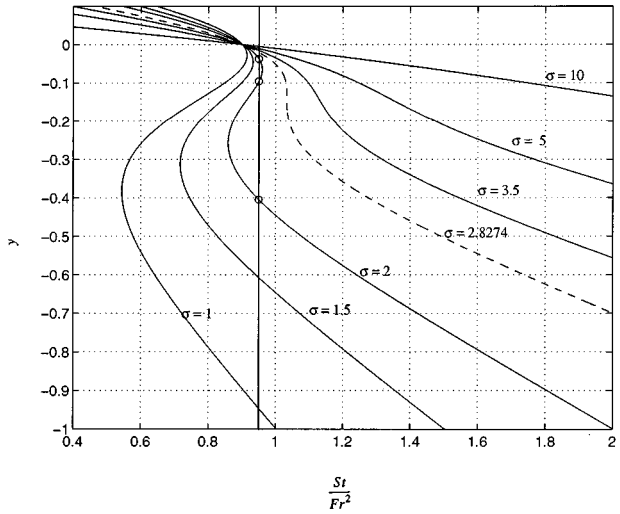

FIG. 4. Equilibrium curves for the vertical set, for $k=0.9$. The intersection(s) of a given St/Fr^2 vertical line with an equilibrium curve corresponding to a given parameter σ value yields the vertical position y of the particle equilibrium point(s).

Figure 4 shows the variation of the left hand side in the second equation in (40) with respect to y, for several values of σ, and $k=0.9$. The intersection of a $\sigma=$const curve, called equilibrium curve, with a vertical line $St/Fr^2=$const yields one or three equilibrium points. As an example, the three equilibrium points resulting from the intersection of the equilibrium curve $\sigma=2.0$ with the vertical line $St/Fr^2=0.95$ are shown. The pattern of the equilibrium curves in Fig. 4 indicates that there is a critical value for σ above which the equilibrium points are always unique, and below which they can be either multiple or unique, depending on the St/Fr^2 value. The value for the critical σ can be found by identifying the curve which has a zero of its first derivative at the same location as a zero of the second derivative.[20] This condition immediately leads to

$$\sigma_{cr}=\pi k, \tag{41}$$

i.e., the critical strain varies linearly with the vorticity distribution parameter. For the curves in Fig. 4, since $k=0.9$, the value for the critical strain parameter is $\sigma_{cr}=2.8274$. The corresponding curve is indicated by a dashed line.

Whether or not particle accumulation at these equilibrium points will occur depends on the stability of these points. In order to perform the stability analysis for the vertical set of equilibrium points, we linearize the velocity field (9),(10) around the equilibrium point from the set, $\mathbf{x_v}=(z_v, y_v)$. Using series expansions along with the z-values in (40) and the values for the vortex center locations $z_0=0.25$ and $z_1=0.75$, the linearized velocity field has the form

$$\begin{aligned} w &= w|_{\mathbf{x_v}} + \frac{2\pi k(-1)^{n+1}\,\sinh(2\pi y_v)}{\cosh^2(2\pi y_v)}\,\zeta, \\ v &= v|_{\mathbf{x_v}} - \left(\frac{2\pi k(-1)^{n+1}\,\sinh(2\pi y_v)}{\cosh^2(2\pi y_v)} + \sigma\right)\eta. \end{aligned} \tag{42}$$

Here (ζ,η) are small displacements around the equilibrium point $\mathbf{x_v}=(z_v, y_v)$. We write the equations (19),(20) for

$z=z_v+\zeta$ and $y=y_v+\eta$, using the velocity field (42), and then subtract from the resulting system the base state equations (19),(20) written for (z_v, y_v), using the velocity field (9),(10) at the point $\mathbf{x_v}=(z_v, y_v)$. The result is a system of four first order ODEs with four unknowns, i.e., the particle's perturbed position (ζ, η) and velocity $(\chi=\dot{\zeta},\ \tau=\dot{\eta})$

$$\begin{bmatrix} \dot{\zeta} \\ \dot{\eta} \\ \dot{\chi} \\ \dot{\tau} \end{bmatrix} = \begin{bmatrix} 0 & 0 & 1 & 0 \\ 0 & 0 & 0 & 1 \\ \dfrac{a}{St} & 0 & -\dfrac{1}{St} & 0 \\ 0 & -\dfrac{a+\sigma}{St} & 0 & -\dfrac{1}{St} \end{bmatrix} \begin{bmatrix} \zeta \\ \eta \\ \chi \\ \tau \end{bmatrix}, \tag{43}$$

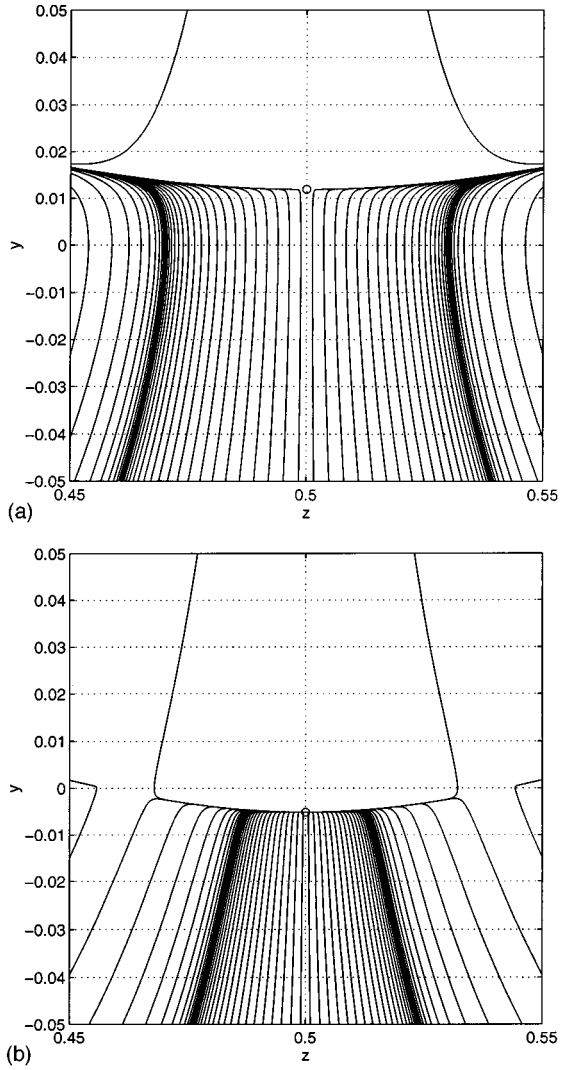

FIG. 5. Modified velocity field. Stability of the equilibrium points from the vertical set for the case when only one equilibrium point may exist. (a) $\sigma=4.0$; $k=0.9$; $St/Fr^2=0.85$. The equilibrium point is located at positive y-coordinate, therefore it is unstable. The pattern of the modified velocity field lines indicates a saddle. (b) $\sigma=4.0$; $k=0.9$; $St/Fr^2=0.92$. The equilibrium point is located at a negative y coordinate, therefore it is stable. The pattern of the modified velocity field lines indicates a node.

where

$$a=\frac{2\pi k(-1)^{n+1}\sinh(2\pi y_v)}{\cosh^2(2\pi y_v)}. \tag{44}$$

The coefficient matrix of the system (43) has eigenvalues of the form

$$\begin{aligned} s_{1,2}&=-\frac{1}{2St}\pm\frac{1}{2St}\sqrt{1+4aSt}, \\ s_{3,4}&=-\frac{1}{2St}\pm\frac{1}{2St}\sqrt{1-4(a+\sigma)St}. \end{aligned} \tag{45}$$

The stability properties determined by the eigenvalues (45) will have to be discussed separately for $n=0$ (even values) and $n=1$ (odd values), corresponding to the downwelling and upwelling regions, respectively. For $n=1$, the solution for y_v from (40) can be either positive or negative. Employing expression (44) for $n=1$ in (45), one obtains

$$\begin{aligned} s_{1,2}&=-\frac{1}{2St}\pm\frac{1}{2St}\sqrt{1+4\frac{2\pi k\sinh(2\pi y_v)}{\cosh^2(2\pi y_v)}St}, \\ s_{3,4}&=-\frac{1}{2St}\pm\frac{1}{2St}\sqrt{1-4\left(\frac{2\pi k\sinh(2\pi y_v)}{\cosh^2(2\pi y_v)}+\sigma\right)St}. \end{aligned} \tag{46}$$

The term $\sinh(2\pi y_v)/\cosh^2(2\pi y_v)$ is positive for $y_v>0$ and negative for $y_v<0$. For positive y_v, the first expression in (46) used with the "+" sign will produce real and positive eigenvalues, thus indicating unstable behavior of the particle. Physically, this is a consequence of the fact that near the equilibrium point the horizontal fluid velocity component points away from this point. For negative y_v, the first expression in (46) may be either real negative, or complex with negative real part. Therefore, in order to check for instability, we have to focus on the second expression $s_{3,4}$. There, the term

$$-\left(\frac{2\pi k\sinh(2\pi y_v)}{\cosh^2(2\pi y_v)}+\sigma\right) \tag{47}$$

is the first derivative of the LHS in the second equation (40), for $n=1$, i.e., the slope of the equilibrium curve. With reference to Fig. 4, the discussion links the eigenvalues $s_{3,4}$ (46) to the slopes of the equilibrium curves. Therefore, when a given equilibrium curve has a negative slope, the term (47) is negative, leading to either complex values with a negative real part, or real negative values in $s_{3,4}$ (46), no matter which sign is chosen, thus indicating stability, provided that $y_v<0$. In the opposite situation, when a given equilibrium curve has positive slope, the term (47) is positive and gives real positive eigenvalues in $s_{3,4}$ (46) with the "+" sign chosen. Thus, the regions with positive slope of the equilibrium curves produce unstable equilibrium points. Such regions exist only if multiple equilibrium points can exist, because only then are the equilibrium curves changing their slopes. Since the positive slope region of the equilibrium curve is confined be-

tween the zeros of the its derivatives, only the middle point of the equilibrium triplets will fall in the unstable region unless the upper equilibrium point has positive vertical coordinate y_v (see Fig. 4, the plotted equilibrium points for $\sigma=2.0$). We also note that for $\sigma>\sigma_{cr}$ there are no positive slopes, therefore the unique equilibrium points are always stable at negative y_v. Note that stability of the particle at a certain equilibrium point does not depend directly on the particle St parameter but only indirectly, as the position of the equilibrium point is determined by the strain σ and the terminal velocity St/Fr^2, and it is the position which determines the stability characteristics.

For $n=0$, corresponding to locations where the fluid is pushed down by the vortices, it was shown above that the equations (40) admit equilibrium points only at negative values of y_v. Consequently, the eigenvalues (45) can be written as

$$s_{1,2}=-\frac{1}{2St}\pm\frac{1}{2St}\sqrt{1+4\left|\frac{2\pi k\,\sinh(2\pi y_v)}{\cosh^2(2\pi y_v)}\right|St},$$

$$s_{3,4}=-\frac{1}{2St}\pm\frac{1}{2St}\sqrt{1-4\left(\left|\frac{2\pi k\,\sinh(2\pi y_v)}{\cosh^2(2\pi y_v)}\right|+\sigma\right)St}. \tag{48}$$

The first expression in (48) with the "+" sign will produce real positive eigenvalues at all positions, hence all equilibrium points for the case in the vertical set are unconditionally unstable. Physically, the horizontal fluid velocity points away from these equilibrium locations, precluding any particle accumulation.

We can summarize the stability discussion for the vertical equilibrium set as follows:

$$\begin{cases} n=1 \text{ upwelling locations} \begin{cases} y_v>0, & \text{unconditionally unstable solutions} \\ y_v\leqslant 0 \begin{cases} \sigma<\sigma_{cr}, & \text{triple equilibrium points may exist. If they do, the middle point is always unstable, the upper point is stable (if located at negative } y_v\text{), and the lower point is stable. If unique, the equilibrium point is stable (if located at negative } y_v, \\ \sigma>\sigma_{cr}, & \text{only unique equilibrium points can exist. If so, they are stable;} \end{cases} \end{cases} \\ n=0 \text{ downwelling locations} \begin{cases} y_v>0, & \text{no solutions,} \\ y_v\leqslant 0, & \text{unconditionally unstable solutions.} \end{cases} \end{cases} \tag{49}$$

In Fig. 5, one can follow the change in the stability characteristics of an equilibrium point in the vertical set as St/Fr^2 is varied. Shown are the streamlines of the modified velocity field for $k=0.9$ and $\sigma=4.0$. Since $\sigma>\sigma_{cr}$, the equilibrium point is unique. In Fig. 5(a), the equilibrium point is still located at positive y_v, and therefore unstable. This is confirmed by the streamlines, which form a saddle. In Fig. 5(b), with $y_v<0$, the equilibrium point is stable, and the streamlines demonstrate the existence of a node.

In Fig. 6, one can follow the change in the stability properties as well as the production and extinction of equilibrium points with increasing gravity, when the strain is subcritical $\sigma<\sigma_{cr}$. Here $k=0.9$ and $\sigma=2.0$. In Fig. 6(a), the influence of gravity is small, and the equilibrium point is displaced only slightly below the stagnation point of the fluid. When gravity is stronger, as for $St/Fr^2=0.89$ in Fig. 6(b), two additional equilibrium points are produced in the vertical set. One can also refer to Fig. 4 and intersect the curve for $\sigma=2.0$ with the appropriate St/Fr^2 vertical line. Note that the upper equilibrium point in the triplet still has a positive y_v-coordinate, and therefore is unstable. Fig. 6(c) shows the points plotted in Fig. 4. Here the upper point of the triplet is located at negative y_v, and therefore stable, while the middle point is an unstable saddle. As gravity increases further, the upper and the middle equilibrium points are displaced towards each other (corresponding to the intersection points of the equilibrium curve for $\sigma=2.0$ in Fig. 4 with a vertical line moving towards the right) until they merge and vanish. Beyond that, only the lowest equilibrium point of the previous triplet is left [Fig. 6(d)]. It is stable, as can be seen from the streamline pattern which indicates a node.

The above discussion demonstrates that a necessary cri-

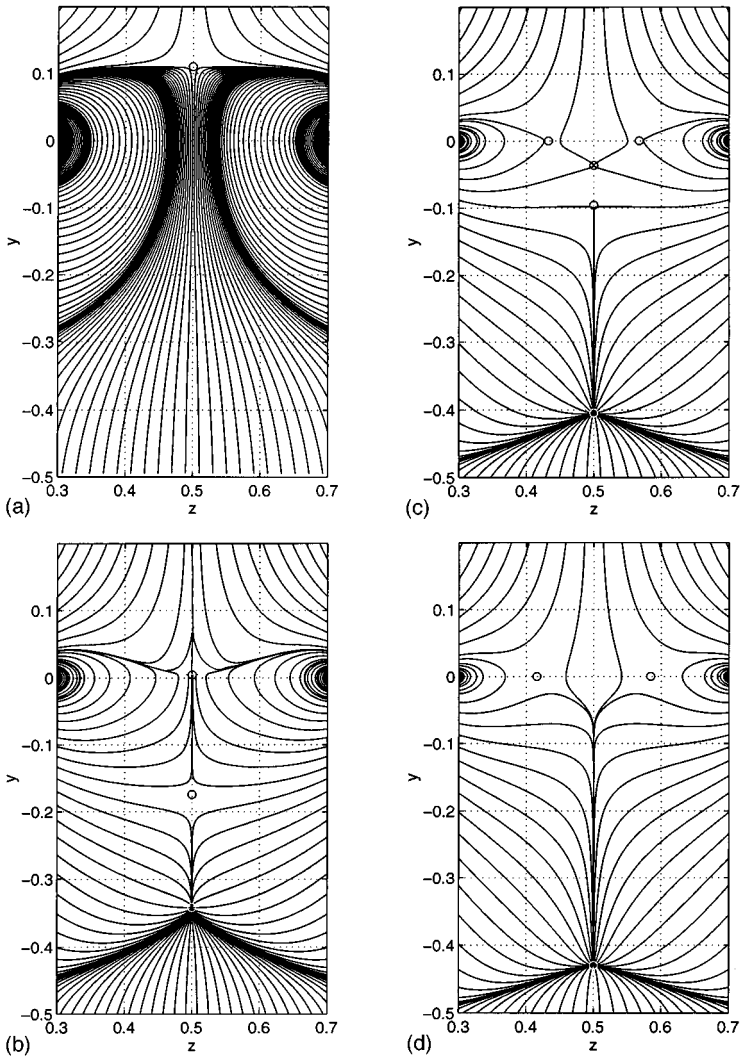

FIG. 6. Modified velocity field. The stability of the equilibrium points from the vertical set. The case when multiple points (triplets) may exist. (a) $\sigma=2.0$; $k=0.9$; $St/Fr^2=0.5$. Single equilibrium point, located at positive y-coordinate and therefore unstable. The pattern of the modified velocity field streamlines indicates a saddle. (b) $\sigma=2.0$; $k=0.9$; $St/Fr^2=0.89$. Three equilibrium points exist: the upper (still located at $y>0$) and the middle one are saddles, while the lower point is a node. (c) $\sigma=2.0$; $k=0.9$; $St/Fr^2=0.95$. Three equilibrium points exist: the upper one is a node, the middle one is a saddle, and the lower one is a node. (d) $\sigma=2,0$; $k=0.9$; $St/Fr^2=0.98$. A single equilibrium point, located at the negative y-coordinate, therefore stable (node). The upper and the middle equilibrium points have merged and vanished.

terion for the accumulation of particles at equilibrium points of the vertical set is the existence in upwelling regions of equilibrium points below the level of the row of counterrotating vortices. This condition $y_v<0$ in the equilibrium equations for the vertical set (40) translates into

$$\frac{St}{Fr^2}>k, \tag{50}$$

which can be considered the fundamental necessary condition for accumulation at the vertical set of equilibrium points.

2. Equilibrium points from the horizontal set

By setting $y=0$ in the second equation of (39), and also using the values $z_0=0.25$ and $z_1=0.75$, one obtains an equation for the locations along the line $y=0$ where equilibrium is achieved. One can then express the horizontal set of equilibrium points in the following form:

$$y_h=0,$$

$$\frac{k\ \cos(2\pi z_h)}{k^2\{1-[\cos(2\pi z_h)]^2\}-1}=\frac{St}{Fr^2}. \tag{51}$$

Along the line $y=0$, the horizontal fluid velocity is zero, whereas the vertical velocity is given by the left hand side term in the second equation in (51). The variation of this velocity as a function of z is plotted in Fig. 7, for several values of k. These curves can again be interpreted as equilibrium curves, similar to Fig. 4 for the vertical set, in the sense that any intersection with a constant level line $St/Fr^2=$const yields the location z_h of an equilibrium point. One can observe in Fig. 7 that, depending on the value of k, either none, two, or four equilibrium points may exist, at locations that are symmetrical with respect to the vertical line $z=0.5$. Due to this symmetry, we will examine only the nature of the equilibrium points located to the left of the

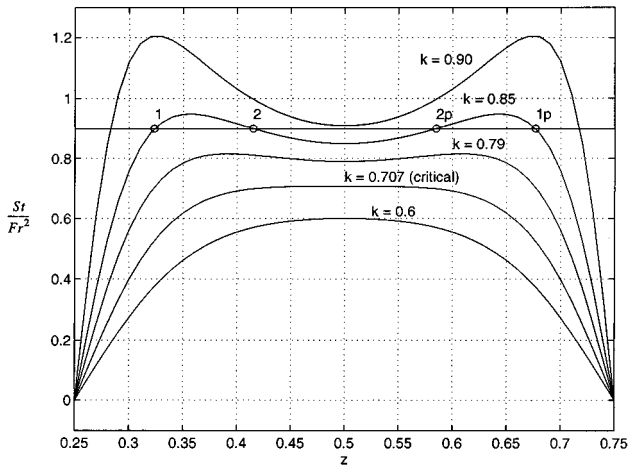

FIG. 7. Equilibrium curves for the horizontal set. The intersection(s) of a given St/Fr^2 horizontal line with an equilibrium curve corresponding to a given parameter k value yields the horizontal position z of the particle equilibrium point(s). The equilibrium points $1p$ and $2p$ are the symmetrical images of the points 1 and 2 with respect to the vertical line $z=0.5$.

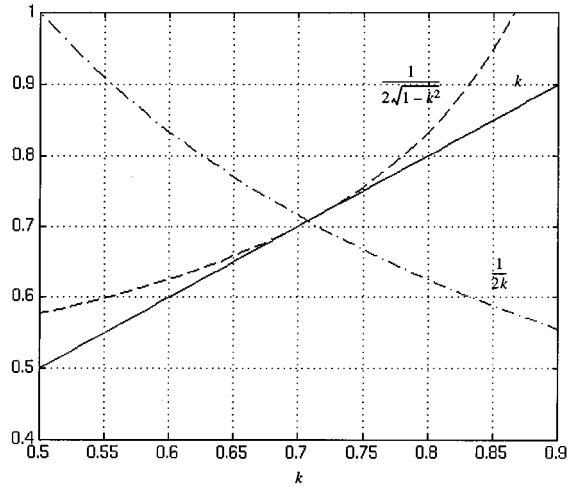

FIG. 8. Variation of various bounds for St/Fr^2 with respect to k.

vertical line $z=0.5$, while keeping in mind that all considerations are valid for the points to the right of it as well.

Whether there are one or two equilibrium points located in the interval $0<z<0.5$ is controlled by the value of k. One can find the critical value of k that separates these two situations by identifying again the curve that has a zero of its first derivative at the same location as a zero of its second derivative.[20] This yields a critical value

$$k_{cr}=\frac{1}{\sqrt{2}} \tag{52}$$

above which two equilibrium points may exist, and below which only one equilibrium point can exist in the horizontal set.

Equation (51) can be cast in a quadratic form for $\cos(2\pi z_h)$ to yield

$$\cos(2\pi z_h)=\frac{-1\pm\sqrt{1-4(1-k^2)(St/Fr^2)^2}}{2k(St/Fr^2)}. \tag{53}$$

Already from equation (51), it follows that in the absence of gravity, when $Fr\to\infty$, and thus $St/Fr^2\to 0$, the equilibrium locations are

$$z_h=\frac{1}{4}\pm m\,\frac{1}{2}, \quad \text{with } m=0,\pm 1,\pm 2,\ldots,$$

which represents the locations of the centers of the counterrotating vortices. In this way, the case without gravity is recovered. Expression (53) provides a condition for a real solution to exist,

$$1-4(1-k^2)\left(\frac{St}{Fr^2}\right)^2\geqslant 0, \tag{54}$$

which leads to a limiting value for St/Fr^2 above which equilibrium points no longer exist in the horizontal set,

$$\frac{St}{Fr^2}\leqslant\frac{1}{2\sqrt{1-k^2}}. \tag{55}$$

Physically, the right hand side of the above inequality expresses the maximum vertical fluid velocity along the line $y=0$. An additional condition for the existence of equilibrium points can be obtained by requiring that the right hand side in (53) be bounded within the interval $[-1,1]$, due to the cosine term on the left hand side. One can easily verify that for values of St/Fr^2 that satisfy (55), the right hand side in (53) taken with the "+" sign is always bounded within $[-1,1]$. However, when the "−" sign is taken, the necessary boundedness is achieved only if

$$\frac{St}{Fr^2}\geqslant\max\left(k,\frac{1}{2k}\right), \tag{56}$$

where the priority in the max function term switches exactly at critical k (given by 52), i.e., above k_{cr}, $k>1/2k$, while below k_{cr}, $k<1/2k$; see Fig. 8.

It was shown above that the "+" sign in (53) corresponds to the vortex center in the absence of gravity. This situation is depicted in Fig. 9(a). As the value of St/Fr^2 increases, gravity gains importance and generates a displacement of the equilibrium point from the position of the vortex center to a different position along the horizontal line $y=0$, as shown in Fig. 9(b). As long as the St/Fr^2 values are below those required by (56), only the "+" sign makes sense in (53) and thus only one equilibrium point will exist. When St/Fr^2 increases enough to satisfy (56), an additional equilibrium point will appear, as shown in Fig. 9(c), corresponding to the "−" sign in (53). The two equilibrium points are further displaced towards each other as St/Fr^2 continues to increase [Fig. 9(d)]. At the limit of inequality (55) the two equilibrium points will merge, and subsequently vanish for larger St/Fr^2 values [Fig. 9(e)].

This scenario is valid for values of k larger than critical, when (55) still allows for (56) to be satisfied. Below k_{cr}, the right hand side in the limiting condition (55) is larger than the right hand side in the condition (56), which means that the condition (56) is no longer active, thus the "−" sign in

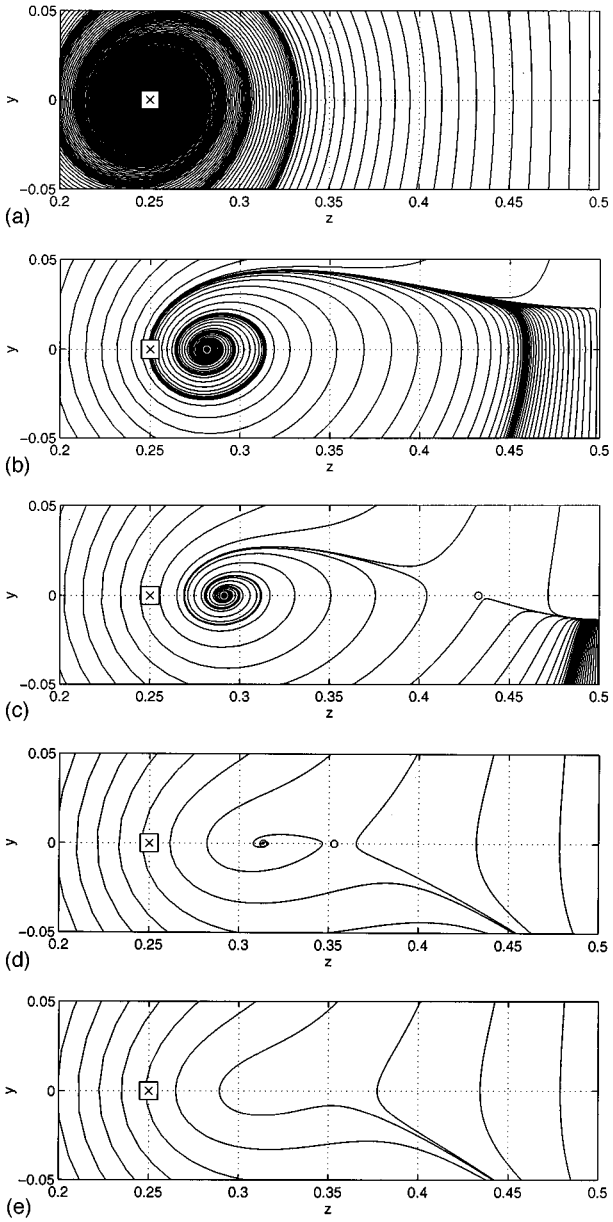

FIG. 9. Modified velocity field. Stability of the equilibrium points from the horizontal set. The case when multiple points (doublets) may exist. (a) $\sigma=4.0$; $k=0.9$; $St/Fr^2=0.0$. No-gravity case; the equilibrium point is located at the vortex center, which is a focus. (b) $\sigma=4.0$; $k=0.9$; $St/Fr^2=0.8$. At weak gravity, the equilibrium point is displaced towards the $z=0.5$ symmetry line. The point is still a focus. (c) $\sigma=4.0$; $k=0.9$; $St/Fr^2=0.95$. For sufficiently strong gravity, a new equilibrium point is created, while the first one is further displaced. The new point is a saddle, while the first one remains a focus. (d) $\sigma=4.0$; $k=0.9$; $St/Fr^2=1.12$. For further increased gravity, the two equilibrium points approach each other towards a merging location. (e) $\sigma=4.0$; $k=0.9$; $St/Fr^2=1.15$. Gravity level is beyond the limit of existence for equilibrium points of the horizontal set. The two points have merged and vanished.

(53) no longer is physically relevant, and only one equilibrium point can exist. In this case, as St/Fr^2 increases, the equilibrium point will be continuously displaced along $y=0$ [Figs. 10(a) and 10(b)] towards the vertical line of symmetry $z=0.5$, where it will merge with its symmetrical counterpart and vanish [Fig. 10(c)].

In order to perform a stability analysis for the horizontal set of equilibrium points, we again linearize the velocity field

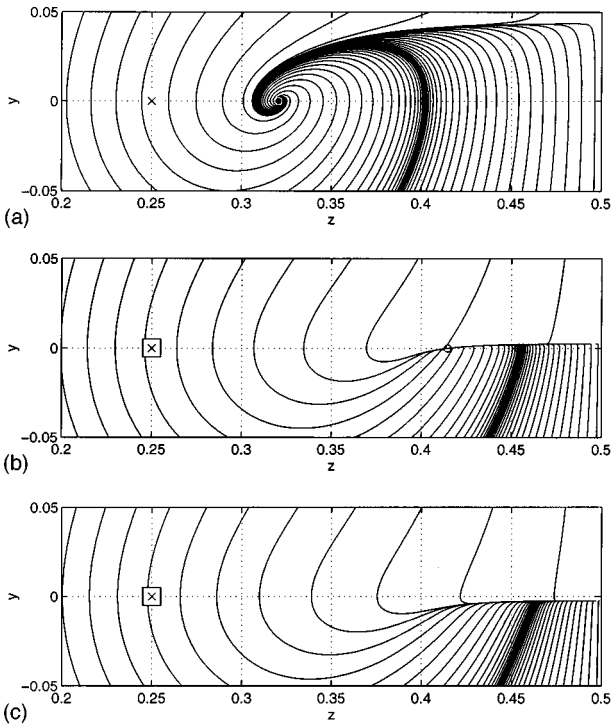

FIG. 10. Modified velocity field. Stability of the equilibrium points from the horizontal set. The case when only one equilibrium point may exist. (a) $\sigma=4.0$; $k=0.7$; $St/Fr^2=0.5$. At weak gravity, the equilibrium point is displaced from its initial location at the vortex center towards the symmetry line $z=0.5$, and remains a focus. (b) $\sigma=4.0$; $k=0.7$; $St/Fr^2=0.69$. The terminal velocity value is close to the k value, the limit of existence for equilibrium points of the horizontal set. The equilibrium point is close to the $z=0.5$ symmetry line and has become a node. (c) $\sigma=4.0$; $k=0.7$; $St/Fr^2=0.71$. The gravity level is beyond the limit of existence of equilibrium points from the horizontal set. The equilibrium point has merged with its symmetrical pair from the right side of the symmetry line $z=0.5$, and vanished.

(9), (10) around the equilibrium point $\mathbf{x_h}=(z_h,y_h)$ from the horizontal set. Using series expansions and setting $y_h=0$, $z_0=0.25$, and $z_1=0.75$, the linearized velocity field has the form

$$w=w|_{\mathbf{x_h}}-\frac{2\pi k\,\sin(2\pi z_h)}{1-k^2\,\sin^2(2\pi z_h)}\,\eta,$$

$$v=v|_{\mathbf{x_h}}+k\pi\left\{\frac{2\sin(2\pi z_h)-k}{(1-k\,\sin(2\pi z_h))^2}+\frac{2\sin(2\pi z_h)+k}{(1+k\,\sin(2\pi z_h))^2}\right\}\zeta, \tag{57}$$

where (ζ,η) are small displacements around the equilibrium point. Performing algebraic manipulations similar to those presented in section III, we obtain a system of four first order ODE's with four unknowns, i.e., the particle's perturbed position (ζ,η) and its velocity $(\chi=\dot{\zeta},\ \tau=\dot{\eta})$,

$$\begin{bmatrix} \dot{\zeta} \\ \dot{\eta} \\ \dot{\chi} \\ \dot{\tau} \end{bmatrix} = \begin{bmatrix} 0 & 0 & 1 & 0 \\ 0 & 0 & 0 & 1 \\ 0 & \frac{b}{St} & \frac{-1}{St} & 0 \\ \frac{c}{St} & \frac{-\sigma}{St} & 0 & \frac{-1}{St} \end{bmatrix} \begin{bmatrix} \zeta \\ \eta \\ \chi \\ \tau \end{bmatrix}, \tag{58}$$

where

$$b = -\frac{2\pi k \sin(2\pi z_h)}{1 - k^2 \sin^2(2\pi z_h)},$$
$$c = k\pi \left\{ \frac{2\sin(2\pi z_h) - k}{(1 - k \sin(2\pi z_h))^2} + \frac{2\sin(2\pi z_h) + k}{(1 + k \sin(2\pi z_h))^2} \right\}. \tag{59}$$

The coefficient matrix of the system (58) has eigenvalues of the form

$$s_{1,2,3,4} = -\frac{1}{2St} \pm \frac{1}{2St} \sqrt{1 - 2\sigma St \pm 2St\sqrt{\sigma^2 + 4bc}}. \tag{60}$$

In spite of the similarity with the no-gravity case (24), the discussion of the stability of the equilibrium points based on the eigenvalues (60) is quite involved, due to the fact that the location appears explicitly in the term $4bc$, so that one cannot easily extract a stability criterion as a function of the particle and flow parameters. The analysis of (60) must be carried out differently for positive and negative values of the expression

$$\Lambda(z_h, k, \sigma) = \sigma^2 + 4bc. \tag{61}$$

As shown in Fig. 11, the dependence of the term $4bc$ on z varies significantly with k, where b and c are given by (59). In addition, the parameter σ can vary widely as well. Nevertheless, the value of Λ divides the interval $0.25 \leqslant z \leqslant 0.5$ into two subintervals. In the left one of these, Λ is negative, while it is positive in the right one. For a fixed σ, the boundary between the two subintervals will be located at different positions for different values of k. Note that the interval $0 \leqslant z \leqslant 0.25$ cannot contain any equilibrium points.

When Λ is negative, all four eigenvalues (60) are complex. Their real parts are

$$Re(s) = -\frac{1}{2St}\left(1 \pm \rho^{1/2} \cos\left(\frac{\theta}{2}\right)\right), \tag{62}$$

where

$$\rho = \sqrt{(1 - 2\sigma St)^2 + 4St^2|\Lambda|} \quad \text{and}$$
$$\theta = \tan^{-1}\left(\frac{2St|\Lambda|}{1 - 2\sigma St}\right). \tag{63}$$

For stability, one requires that $Re(s) \leqslant 0$. Using (63) and again the trigonometric relation (27), one obtains the stability condition

$$St < \frac{2\sigma}{|\Lambda(z_h, k, \sigma)|}. \tag{64}$$

Consequently, in this case the stability of the equilibrium point $(z_h, y_h = 0)$ depends explicitly on St, σ, and k, but not on the parameter St/Fr^2. The situation is similar to that of a Burgers vortex[20] in the presence of gravity, in that the terminal velocity St/Fr^2 determines the location of the equilibrium point, while not directly entering into the related stability criterion (64).

When Λ is positive, the eigenvalues (60) may be either real or complex, depending on the sign of the expression under the outer square root. In this case, complex eigenvalues indicate stability, since the real part will be negative. One can write the expression (60) in the form

$$s_{1,2,3,4} = -\frac{1}{2St}\left(1 \pm \sqrt{1 - 2St(\sigma \pm \sqrt{\Lambda})}\right). \tag{65}$$

By analyzing (65), one obtains that if $\sigma - \sqrt{\Lambda} > 0$ the eigenvalues are either complex with a negative real part, or real and negative, thus indicating stability. On the other hand, if $\sigma - \sqrt{\Lambda} < 0$ at least one of the four eigenvalues will be real and positive, thus indicating instability. Along with (61), this condition translates into stability for $4bc < 0$, and instability for $4bc > 0$. One can see in Fig. 11 that the curves $4bc$ either stay negative for the whole interval $0.25 \leqslant z_h \leqslant 0.5$ if $k < k_{cr}$, or become positive towards the right end of the interval for values $k > k_{cr}$. In this latter case, the zero-crossing coordinate is always given by the solution of (53) at the limit of condition (55), so that the zero-crossing takes place at the location where the two equilibrium points merge and vanish.

Consequently, the stability conditions for the equilibrium points of the horizontal set can be summarized as follows:

$$\Lambda(z_h, k, \sigma) < 0, \quad \begin{cases} St < \dfrac{2\sigma}{|\Lambda(z_h, k, \sigma)|}, & \text{stable equilibrium points,} \\ St > \dfrac{2\sigma}{|\Lambda(z_h, k, \sigma)|}, & \text{unstable equilibrium points;} \end{cases} \tag{66}$$

$$\Lambda(z_h, k, \sigma) > 0, \quad \begin{cases} 4bc < 0, & \text{stable equilibrium points,} \\ 4bc > 0, & \text{unstable equilibrium points.} \end{cases}$$

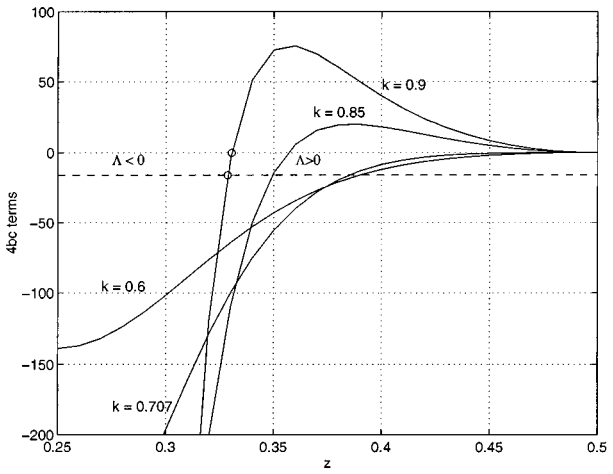

FIG. 11. The variation of the term $4bc$ with respect to k. For values $k>k_{cr}$, the curves have a positive region towards the right of the interval, otherwise they remain negative. Also shown are the points of zero-crossing and the boundary point between $\Lambda<0$ and $\Lambda>0$ for $k=0.9$ and $\sigma=4.0$.

A physical interpretation of these results may again be obtained by describing the evolution of the location and stability of the equilibrium point(s) with increasing gravity. In the absence of gravity, the only equilibrium point from the horizontal set is located at the center of the vortex. At this location, substituting $z_h=0.25$ into (66), the term $4bc$ becomes $-4(2\pi k/(1-k^2))^2=-4\phi^2(k)$ [see (23)], which is negative, and condition (66) reduces to (31). As we pointed out for the no-gravity case, an important condition for stability at the center of the vortex is the existence of strong strain, i.e., large σ. Consequently, without gravity one equilibrium point exists, which is located at the center of the vortex, and whose stability is determined by (31). The streamline pattern in Fig. 9(a) shows that the equilibrium point has the form of a focus.

As gravity increases, the equilibrium point is continuously shifted towards the right along the line $y=0$. For $k=0.9>k_{cr}$ and $\sigma=4.0$ as in Fig. 10, the term $4bc$ is negative over the interval $0.25\leqslant z_h\leqslant 0.3305$ (see Fig. 11), and $\Lambda<0$ over the interval $0.25\leqslant z_h\leqslant 0.3285$. Therefore, over this last interval, the stability is controlled by the first set of conditions in (66). For $k=0.7<k_{cr}$ and $\sigma=4.0$ as in Fig. 11, the term $4bc$ is always negative, while Λ is negative over the interval $0.25\leqslant z_h\leqslant 0.3855$, so that over this interval the stability of the particle at the equilibrium point is governed by the first set of conditions in (66) as well. In both cases the equilibrium point is a focus, and its stability depends explicitly on the particle St value.

When gravity is increased sufficiently for condition (56) to be satisfied, a second equilibrium point will appear if $k>k_{cr}$. This occurs between the situation shown in Fig. 9(b) and that shown in Fig. 9(c). To find the new equilibrium point's location, one can substitute $St/Fr^2=k$ into equation (53) taken with the ("$-$") sign. This yields $z_h=0.5$, i.e., the right border of the interval considered. At this location, $4bc=0$, so that Λ is positive and the equilibrium point is neutrally stable. For $k<k_{cr}$ no additional equilibrium points appear, since for subcritical k the limiting conditions (55) and (56) cannot be satisfied simultaneously, so that a second solution for equation (53) does not exist.

As gravity increases further, for $k>k_{cr}$ the initial equilibrium point will continue to move towards the right, while the additional point will start to move towards the left. This can be shown either by solving (53) for increasing St/Fr^2, or by following in Fig. 7 the intersections of a curve corresponding to $k=0.9$ with a horizontal line moving upwards. As soon as the second equilibrium point leaves the $z_h=0.5$ position, it becomes unstable. For the case $k=0.9$ and $\sigma=4.0$, the term $4bc>0$ near the right border of the interval (see Fig. 11). With $z_h>0.3285$, we have $\Lambda>0$, so that the stability of the second equilibrium point is governed by the second set of conditions in (66) which indicates instability. This is evident in Figs. 9(c) and 9(d), as the streamlines form a saddle at the new equilibrium point's location. The initial equilibrium point is still a focus at this level of gravity.

If gravity increases further, the two equilibrium points will collide for supercritical k once the level of gravity given by the limit of condition (55) is reached. The collision happens at the zero-crossing of the $4bc$ term, which is $z_h=0.3305$ for $k=0.9$ and $\sigma=4.0$. For $k<k_{cr}$, the single equilibrium point will become unconditionally stable as it passes the boundary between $\Lambda<0$ and $\Lambda>0$, which is located at $z_h=0.3855$ for the case in Fig. 11. As shown in Fig. 10(b), the point then corresponds to a node. Subsequently, the equilibrium point will collide with its symmetrical pair to the right of the vertical line $z=0.5$. This collision occurs at the intersection of the $y=0$ line with the $z=0.5$ line.

For gravity levels larger than that the limit of (55), only equilibrium points from the vertical set are possible. If the strain is strong enough to enforce the condition $\sigma>\sigma_{cr}$, only one stable equilibrium point exists in the entire flow field.

It is of interest to note that for $k>k_{cr}$ the stability properties of the first equilibrium point change during the last part of its motion along $y=0$, just before the collision. By examining Fig. 11, one can observe that in order to reach the collision location $z_h=0.3305$, the left equilibrium point must pass the boundary between the negative Λ and positive Λ, $z_h=0.3285$. Once this boundary is passed, the term $4bc$ is still negative, but Λ is positive, indicating unconditional stability according to (66). Thus, the initial equilibrium point has a range of locations where it is stable regardless of the value of St. The interval is bounded by the zero-crossing location of Λ to the left, and by the zero-crossing location of $4bc$ to the right (see Fig. 11, for $k=0.9$).

B. Gravity pointing in the spanwise direction

Here we consider flows for which gravity points in the negative z-direction. This results in $e_{gz}=-1$, $e_{gy}=0$ in equations (19) and (20). Proceeding in a manner similar to the above, one obtains a system of two equations with two unknowns for the equilibrium locations,

$$-0.5\,\frac{\sinh[2\pi(y-y_0)]}{\cosh[2\pi(y-y_0)]-k\,\cos[2\pi(z-z_0)]}$$

$$+0.5\,\frac{\sinh[2\pi(y-y_1)]}{\cosh[2\pi(y-y_1)]-k\,\cos[2\pi(z-z_1)]}-\frac{St}{Fr^2}=0, \tag{67}$$

$$0.5\,\frac{k\,\sin[2\pi(z-z_0)]}{\cosh[2\pi(y-y_0)]-k\,\cos[2\pi(z-z_0)]}$$

$$-0.5\,\frac{k\,\sin[2\pi(z-z_1)]}{\cosh[2\pi(y-y_1)]-k\,\cos[2\pi(z-z_1)]}-\sigma y=0.$$

In the following, we provide a brief analysis of the equilibrium point locations and their stability, based on the modified velocity field plots.

The presence of a spanwise component of the gravity vector destroys the symmetry of the streamline pattern of the modified flowfield, as shown in Fig. 12(a). The equilibrium points are displaced from their no-gravity position in both their z- and y-coordinates, while maintaining their nature as pairs of foci and saddle points. As gravity increases, the focus and saddle move closer to each other, as shown in Fig. 12(b), until they collide and vanish. Fig. 12(c) shows the case when the terminal velocity St/Fr^2 is larger than the maximum horizontal fluid velocity, for which equilibrium points no longer exist.

The observation of main interest is that for the present orientation of gravity there are no unconditionally stable accumulation points, i.e., no nodes in the modified stream-line pattern. For low values of gravity, conditionally stable accumulation points in the form of foci exist, whereas for stronger values of gravity no equilibrium points are present. As a necessary condition for the existence of conditionally stable accumulation points in the flow, the terminal velocity must be smaller than the maximum z-component of the fluid velocity. This leads to

$$\frac{St}{Fr^2}<\frac{k}{2\sqrt{1-k^2}}. \tag{68}$$

C. Arbitrary orientation of the gravity vector in the cross-stream plane

In this most general case, gravity forms an angle α with the $-y$-direction, so that there are gravitational components acting both in the z- and in the y-direction. Here, we assume that the gravity components act in $-z$ and $-y$-direction, respectively, hence $e_{gz}=-\sin(\alpha)$, and $e_{gy}=-\cos(\alpha)$. Consequently, each of the equations (19), (20) retains a term related to gravity. The equilibrium equations, obtained from (19), (20) with the flowfield (9), (10) form a system of two equations for two unknowns,

$$0.5\,\frac{\sinh[2\pi(y-y_0)]}{\cosh[2\pi(y-y_0)]-k\,\cos[2\pi(z-z_0)]}$$

$$+0.5\,\frac{\sinh[2\pi(y-y_1)]}{\cosh[2\pi(y-y_1)]-k\,\cos[2\pi(z-z_1)]}$$

$$+\frac{St}{Fr^2}\,e_{gz}=0,$$

$$0.5\,\frac{k\,\sin[2\pi(z-z_0)]}{\cosh[2\pi(y-y_0)]-k\,\cos[2\pi(z-z_0)]} \tag{69}$$

$$-0.5\,\frac{\sinh[2\pi(z-z_1)]}{\cosh[2\pi(y-y_1)]-k\,\cos[2\pi(z-z_1)]}-\sigma y$$

$$+\frac{St}{Fr^2}\,e_{gy}=0.$$

The above equations must be solved numerically in order to obtain the positions (z_e, y_e) of the equilibrium points. Stability of these equilibrium points then requires that the local fluid velocity field, after subtraction of the terminal settling velocity, has the character of a stable fixed point.

A general linear linear stability analysis around a generic equilibrium point can be carried out in a manner similar to the analyses presented in sections III and IV A. By using series expansions around a generic equilibrium point $\mathbf{x_e}=(z_e, y_e)$ one can express the fluid velocities as

$$w=w|_{\mathbf{x_e}}+\epsilon\,\frac{\partial w}{\partial z}+\eta\,\frac{\partial w}{\partial y},$$

$$v=v|_{\mathbf{x_e}}+\epsilon\,\frac{\partial v}{\partial z}+\eta\,\frac{\partial v}{\partial y}, \tag{70}$$

where (ϵ,η) are small displacements around the equilibrium point. These linearized expressions for the fluid velocity field (70), after some algebraic manipulations similar to those in sections III and IV A, lead to a system of four first order ODE's with four unknowns, i.e., the particle perturbed position (ϵ,η) and velocity $(\chi=\dot{\epsilon},\ \tau=\dot{\eta})$,

$$\begin{bmatrix}\dot{\epsilon}\\ \dot{\eta}\\ \dot{\chi}\\ \dot{\tau}\end{bmatrix}=\begin{bmatrix}0 & 0 & 1 & 0\\ 0 & 0 & 0 & 1\\ \frac{a}{St} & \frac{b}{St} & \frac{-1}{St} & 0\\ \frac{c}{St} & \frac{d}{St} & 0 & \frac{-1}{St}\end{bmatrix}\begin{bmatrix}\epsilon\\ \eta\\ \chi\\ \tau\end{bmatrix}, \tag{71}$$

where $a=\partial w/\partial z$, $b=\partial w/\partial y$, $c=\partial v/\partial z$, $d=\partial v/\partial y$ are the components of the fluid velocity gradient tensor. The eigenvalues of the coefficient matrix in the system (71) are

$$s_{1,2,3,4}=\frac{1}{St}\,[-1\pm\sqrt{1+St(a+d\pm\sqrt{(a-d)^2+4bc})}]. \tag{72}$$

These eigenvalues (72) allow us to identify those regions in the flowfield in which any existing equilibrium points would be unconditionally stable. One can immediately observe that if expression $\Lambda=(a+d\pm\sqrt{(a-d)^2+4bc})$ in (72)

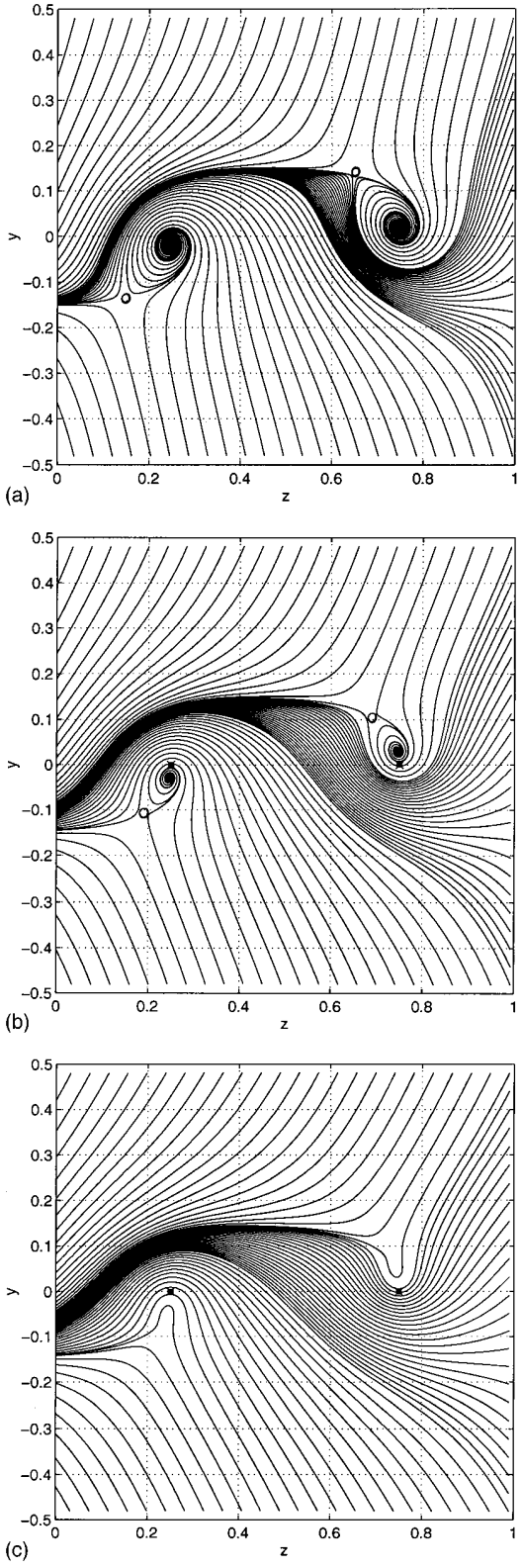

FIG. 12. Modified velocity field for the case of the vertical row of vortices. Here gravity acts from right to left. The black dots mark the center of the vortices, while the circles mark the position of the equilibrium points, if they exist (a) $\sigma=4.0$; $k=0.9$; $St/Fr^2=0.5$. Gravity destroys the symmetry of the line pattern. The equilibrium points are displaced from both their no-gravity case z-and y-coordinates. The line pattern suggest two sets of focus-saddle points. (b) $\sigma=4.0$; $k=0.9$; $St/Fr^2=0.75$. Increasing gravity does not generate any additional equilibrium points. The initial stability characteristics remain the same, while the points in each focus-saddle pair move closer to each other. (c) $\sigma=4.0$; $k=0.9$; $St/Fr^2=1.0$. After collision, all equilibrium points vanish. Gravity is strong enough to ''wash'' out all of the equilibrium points.

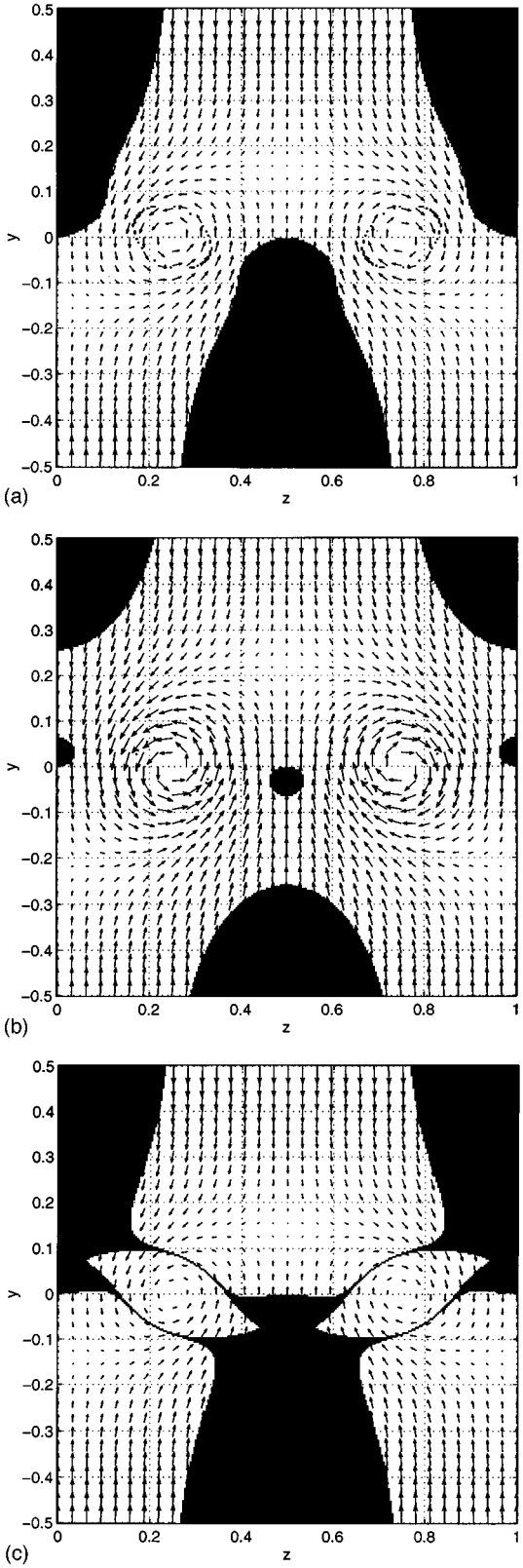

FIG. 13. The topology of the zones of potential particle accumulation. (a) $\sigma=4.0$; $k=0.9$. The zones corresponding to potential particle accumulation (dark areas) are located at the up- and downwelling locations, alternatively. (b) $\sigma=2.0$; $k=0.9$. The zones corresponding to potential particle accumulation (dark areas) have become disconnected: one small area, located close to the vortex row line and one larger area can be observed at each down- and upwelling location. (c) $\sigma=4.0$; $k=0.8$. The zones corresponding to potential particle accumulating (dark areas) located at downwelling locations have become connected to the areas located at upwelling locations.

is real and negative, then the eigenvalues are either real and negative, or complex with negative real part, both of which cases indicate unconditional stability.

Figure 13 distinguishes areas where the term Λ is real and negative (dark areas) from those where it is either real and positive or complex (white areas). The dark areas indicate zones of unconditional stability, provided that equilibrium points are located within those zones. These zones of unconditional stability do not depend on the particle characteristics (St), but only on the flow characteristics. Their topology changes, as the strain coefficient σ or the Stokes' parameter k are varied. In Fig. 13(a), for $\sigma=4$ and $k=0.9$, the zones of unconditional stability are periodically located in the up- and downwelling flow areas. For a lower value of $\sigma=2$, a small island of unconditional stability survives near the vortex row. This is shown in Fig. 13(b), which also provides a better understanding of the stability characteristics for the vertical set of equilibrium points in Fig. 6. An interesting topology develops when $\sigma=4$ and the Stokes' parameter is lowered to $k=0.8$. The unconditionally stable zones in the down-welling regions become linked to those in the upwelling regions by thin filaments around the cores of the counterrotating vortices.

V. CONCLUSIONS

The present investigation represents a first step towards extending results for particle accumulation and dispersion in two-dimensional free shear flows to fully three-dimensional flows. A prominent feature of these three-dimensional flows, absent in two dimensions, is the existence of stretched vortices. These were shown earlier[20] to possess the ability to trap heavy particles. Consequently, the array of extensionally strained counterrotating vortices known to exist in the braid region of three-dimensionally evolving mixing layers, can be expected to significantly affect the dynamics of the bands of heavy particles forming there as a result of the action of the spanwise Kelvin-Helmholtz rollers. In order to be able to make theoretical progress, we employ an analytical model for the fluid flow in the braid region, based on Stuart vortices. This approach allowed us to identify the locations of equilibrium points for the heavy particles. By employing some basic tools from the field of dynamical systems theory, we were able to demonstrate the existence of both unstable (saddle), conditionally stable (foci), and unconditionally stable (nodes) equilibrium points. The latter two may serve as accumulation regions for the heavy particles. Accumulation criteria were derived in terms of the particle St and Fr numbers, and the flow parameters.

In the absence of gravity, accumulation of moderate St particles can occur only at the center of the braid vortices. An analytical expression for the critical particle diameter, below which accumulation is possible, was derived. The effect of gravity can lead to the emergence of multiple equilibrium points, whose stability properties depend on their locations. Orientations of the gravity vector both perpendicular to and within the plane of the mixing layer were considered. In the former case, unconditional accumulation is possible only midway between the streamwise braid vortices in the upwelling regions, if gravity is strong enough to create equilibrium points below the plane of the mixing layer. Conditionally stable accumulation regions exist a short horizontal distance away from the centers of the braid vortices. If the gravity vector lies within the plane of the mixing layer, accumulation points exist only for moderate values of Fr. Under these conditions, conditional accumulation is possible near the streamwise vortex centers.

The above results only concern the existence and stability of equilibrium points. They cannot address such issues as, for example, the size of the basin of attraction of the stable equilibrium points, or the nonlinear dynamics of particles for which stable equilibrium points do not exist. Finding answers to these questions requires the help of numerical simulations, which will be discussed in detail in Part 2 of the present investigation.[21] There we will explore the *nonlinear* dynamics of heavy particles in the braid region of the mixing layer, in order to study the potential accumulation of particles on equilibrium trajectories, along with the characteristic features of the related particle concentration fields.

ACKNOWLEDGMENTS

The authors gratefully acknowledge support by the National Science Foundation under Grant No. CTS-9196004, and by the Electric Power Research Institute. Computing resources were provided by the San Diego Supercomputer Center.

[1] G. L. Brown and A. Roshko, "On density effects and large structure in turbulent mixing layers," J. Fluid Mech. **64**, 775 (1974).
[2] C. D. Winant and F. K. Browand, "Vortex pairing: The mechanism of turbulent mixing layer growth at moderate Reynolds numbers," J. Fluid Mech. **63**, 237 (1974).
[3] C. T. Crowe, R. A. Gore, and T. R. Troutt, "Particle dispersion by coherent structures in free shear flows," Part. Sci. Technol. **3**, 149 (1985).
[4] J. N. Chung and T. R. Troutt, "Simulation of particles in an axisymmetric jet," J. Fluid Mech. **186**, 199 (1988).
[5] F. Wen, N. Kamalu, J. N. Chung, C. T. Crowe, and T. R. Troutt, "Particle dispersion by vortex structures in plane mixing layers," ASME J. Fluids Eng. **114**, 657 (1992).
[6] J. E. Martin and E. Meiburg, "The accumulation and dispersion of heavy particles in forced two-dimensional mixing layers. Part 1: The fundamental and subharmonic cases," Phys. Fluids **6**, 1116 (1994).
[7] N. Raju and E. Meiburg, "The accumulation and dispersion of heavy particles in forced two-dimensional mixing layers. Part 2: The effect of gravity," Phys. Fluids (in press).
[8] B. J. Lazaro and J. C. Lasheras, "Particle dispersion in a turbulent, plane, free shear layer," Phys. Fluids A **1**, 1035 (1989).
[9] B. J. Lazaro and J. C. Lasheras, "Particle dispersion in the developing free shear layer. Part 1: Unforced flow," J. Fluid Mech. **235**, 143 (1992).
[10] B. J. Lazaro and J. C. Lasheras, "Particle dispersion in the developing free shear layer. Part 2: Forced flow," J. Fluid Mech. **235**, 179 (1992).
[11] E. K. Longmire and J. K. Eaton, "Structure and control of a particle-laden round jet," J. Fluid Mech. **236**, 217 (1992).
[12] K. T. Kiger and J. C. Lasheras, "Effect of vortex pairing on particle dispersion and kinetic energy transfer in a two-phase turbulent shear layer," J. Fluid Mech. **302**, 149 (1995).
[13] L. P. Bernal and A. Roshko, "Streamwise vortex structures in plane mixing layers," J. Fluid Mech. **170**, 499 (1986).
[14] W. T. Ashurst and E. Meiburg, "Three dimensional shear layers via vortex dynamics," J. Fluid Mech. **189**, 87 (1988).
[15] J. C. Lasheras and H. Choi, "Three-dimensional instability of a plane, free shear layer: An experimental study of the formation and evolution of streamwise vortices," J. Fluid Mech. **189**, 53 (1988).
[16] G. M. Corcos and S. J. Lin, "The mixing layer: Deterministic models of a turbulent flow. Part 2. The origin of the three-dimensional motion," J. Fluid Mech. **139**, 67 (1984).
[17] S. J. Lin and G. M. Corcos, "The mixing layer: Deterministic models of a

turbulent flow. Part 3. The effect of plane strain on the dynamics of streamwise vortices,'' J. Fluid Mech. **141**, 139 (1984).
[18]J. C. Neu, ''The dynamics of stretched vortices,'' J. Fluid Mech. **143**, 253 (1984).
[19]J. M. Burgers, ''A mathematical model illustrating the theory of turbulence,'' Adv. Appl. Mech. **1**, 171 (1948).
[20]B. Marcu, E. Meiburg, and P. K. Newton, ''Dynamics of heavy particles in a Burgers vortex,'' Phys. Fluids **7**, 400 (1995).
[21]B. Marcu and E. Meiburg, ''The effect of the streamwise braid vortices on the particle dispersion in a plane mixing layer. II. Nonlinear particle dynamics,'' Phys. Fluids **8**, 734 (1996).
[22]J. T. Stuart, ''On finite amplitude oscillations in laminar mixing layers,'' J. Fluid Mech. **29**, 417 (1967).
[23]R. Mallier and S. A. Maslowe, ''A row of counter-rotating vortices,'' Phys. Fluids A **5**, 1074 (1993).
[24]G. M. Corcos and F. S. Sherman, ''The mixing layer: Deterministic models of a turbulent flow. Part 1. Introduction and the two-dimensional flow,'' J. Fluid Mech. **139**, 29 (1984).
[25]M. R. Maxey and J. J. Riley, ''Equation of motion for a small rigid sphere in a nonuniform flow,'' Phys. Fluids **26**, 883 (1983).
[26]R. Clift, J. R. Grace, and M. E. Weber, *Bubbles, Drops and Particles* (Academic Press, New York, 1978).
[27]J. H. Bell and R. D. Mehta, ''Measurements of the streamwise vortical structures in a plane mixing layer,'' J. Fluid Mech. **239**, 213 (1992).
[28]A. M. Gañan Calvo and J. C. Lasheras, ''The dynamics and mixing of small spherical particles in a plane, free shear layer,'' Phys. Fluids A **3**, 1207 (1991).